2016-01-01

3-D Structure of Colombia From 1-D Constrained Joint Inversion Of Receiver Functions and Surface Wave Dispersion

Nick Talavera
University of Texas at El Paso, contact@nicktalavera.com

3-D STRUCTURE OF COLOMBIA FROM 1-D CONSTRAINED JOINT INVERSION OF RECEIVER FUNCTIONS AND SURFACE WAVE DISPERSION

NICHOLAS ALEXANDER TALAVERA

Master's Program in Geophysics

APPROVED:

Aaron Velasco, Ph.D., Chair

Laura Serpa, Ph.D.

Harold Gurrola, Ph.D.

Charles Ambler, Ph.D.

Dean of the Graduate School

3-D STRUCTURE OF COLOMBIA FROM 1-D CONSTRAINED JOINT INVERSION OF RECEIVER FUNCTIONS AND SURFACE WAVE DISPERSION

by

NICHOLAS ALEXANDER TALAVERA, BACHELOR OF SCIENCE

THESIS

Presented to the Faculty of the Graduate School of

The University of Texas at El Paso

in Partial Fulfillment

of the Requirements

for the Degree of

MASTER OF SCIENCE

Department of Geosciences

THE UNIVERSITY OF TEXAS AT EL PASO

May 2016

ACKNOWLEDGEMENTS

First and foremost, I would like like to thank my father for supporting me throughout my academic career. I would like to thank Dr. Aaron Velasco for offering his mentorship and his guidance. I would also like to thank Dr. Velsaco for introducing me to Cyber-Share, the program that has been welcoming to me and offered me financial support in my final semester. I would like to thank Dr. Laura Serpa for finding me opportunities and being a person I could always count on to give me sound advice. I would like to thank Dr. Harold Gurrola for his continued guidance and friendship. I would like to thank Anibal Sosa for his work on joint inversions on my project

TABLE OF CONTENTS

LIST OF TABLES

LIST OF EQUATIONS

LIST OF FIGURES

INTRODUCTION

The country, Colombia, resides at the northwest corner of the South America with seismicity and volcanism due to the intersections of the Nazca, South America and Caribbean tectonic plates (Figure 1). The boundaries of the South America plate, on which Colombia lies, borders between 60 to 200 kilometers from its coasts. A dense spot of seismicity known as the Bucaramanga Nest has had many theories to explain its existence. Two tectonic microplates suspected in this region have not been well understood. With many mysteries of the behavior of the tectonic plates beneath Colombia, using new methods may shed light on some of these controversies.

We need to generate models of the crust and mantle to examine these plates. To make that model, we can calculate 1-D joint inversion models that combine receiver functions and surface wave dispersion tomography which will be useful in this application due to their complementary ability to study velocities. A new method to calculate receiver functions by adjusting back azimuth rotations will be used.

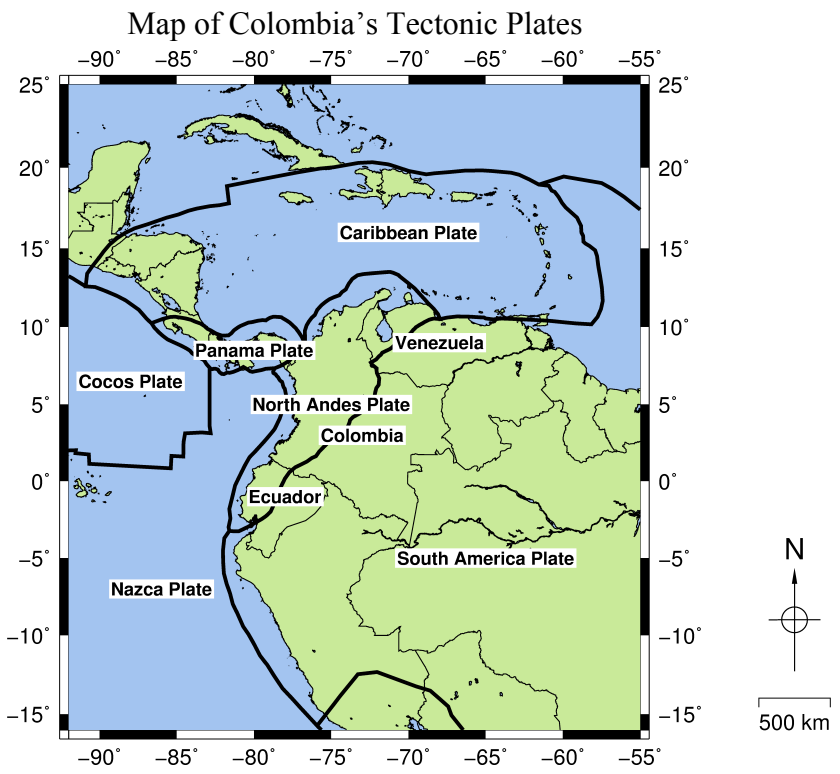

Figure 1: Map of Colombia's Tectonic Plates. This map uses tectonic plate boundaries from Bird (2003). The Caribbean plate subducts beneath the North Andes plate and acts as a transform boundary with the South America plate above Venezuela. The Nazca plate subducts beneath the North Andes and South America plate. The Cocos, Nazca and Caribbean Plate subduct beneath the the Panama plate. The South America plate subducts horizontally underneath the North Andes plate.

TECTONIC SETTING

Colombia lies in a tectonically complex region of the world. The Caribbean plate meets the South America plate at an east-west striking transform boundary north of Colombia (Figure 1). The Caribbean microplate subducts beneath the North Andes plate boundary transitions at a convergent boundary towards the west of the transform boundary, above Venezuela (USGS, 2012).

The Nazca plate subducts beneath the South America plate boundary along the Pacific Ocean at Colombia's coast. Convergence shifts the Nazca plate northeastward at ~70 mm/year (USGS , 2012). Seismicity has been used to find that the Nazca plate subducts at about 35° in the southeast direction in the Benioff-Wadati zone (Pennington, 1981).

The North Andes microplate spans northwest Colombia and Venezuela bounded by the northern portion of the Andes mountains and constrained by the Caribbean and Nazca Plates. The Nazca plate plate subducts beneath the North Andes microplate, and the North Andes microplate subducts beneath the Caribbean plate (Allenby, 1984; Freymueller, et al., 1993). The North Andes - South America plate boundary appears to be a combination of a transform boundary and a horizontal subduction of the South America plate but there have been disagreements of whether it behaves exclusively as either one of these or both (Allenby, 1984; Bird, 2003; Freymueller, et al., 1993).

The Panama microplate lies between the Cocos, Nazca, South America, and Caribbean plates (Bird, 2003). The Nazca plate, the Caribbean plate, and the Cocos subduct beneath the Panama plate (Mann, 1995).

An area at 6.8°N and 73.1°W in central Colombia has a concentrated occurrence of 150 to 200 km depth earthquakes and has been named The Bucaramanga Nest (Prieto, et al., 2013;

Zarifi, et al., 2007). There have been 80,000 earthquakes in the area since 1993 with a magnitude 4 quake “every month or so” (Prieto, et al., 2013). This nest may exist due to contacting slabs, two overlapping slabs, or extreme bending of a single slab, but there has not been a consensus among seismologists for the tectonic interpretation of this nest.

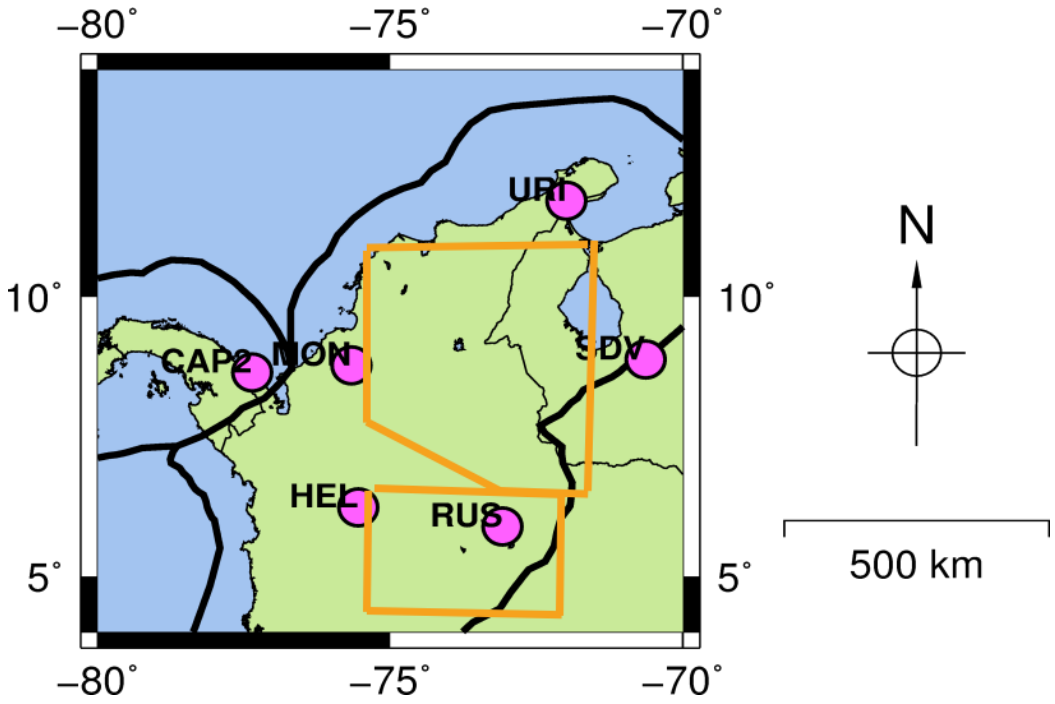

Figure 2: This map has the the northern and southern slab as approximated from Zarifi et al. (2007) overlaid on a map of Colombia. The stations used are labeled as purple circles with their station names.

According to Prieto et al. (2013), the Bucaramanga Nest could be active due to crustal failure in the mantle due to substantial shear heating and partial melting along with the collision of the two plates. Zarifi et al. (2007) studied a southern slab from 75°W to 72°W slab that subducts down to about 300km deep that dips at 29°. This southern slab has been colliding at 5° N with a northern slab that dips at 50° in the south at the tear and increases to 25° in the north (Zarifi, et al., 2007).

Vargas & Mann (2013) proposed the presence of a southeast dipping lithospheric slab, nicknamed the "Caldas slab tear," subducting in the Benioff zone beneath Colombia (Vargas & Mann, 2013). Their research suggests the existence of a 240 km long, narrow, east–west trending tear between the boundary of two subducted slabs of different dips, which formed as a zone of lithospheric weakness along the subducted part of the inactive Sandra spreading ridge.

Pennington (1981) has suggested the presence of a northeast dipping plate that would dip downwards at 35° off the coast of Ecuador. Allenby (1984) proposes that this may be a separate plate due a tear due to the presence of another separate 10° dipping plate just south near Peru that appears to have resulted from a tear.

A map of seismicity in Colombia that has been colored correspond to the hypocenter depth can be seen in Figure 2. There has been relatively infrequent 0-33km depth seismicity along the Caribbean-South America plate boundary compared to the rest of the boundaries probably due to its behavior as a transform plate boundary. Earthquakes at the Nazca–South America plate boundary tend to be shallow, 0-33km deep, increasing to 150-300km deep at about 300km away from the boundary towards the center of the South America plate.

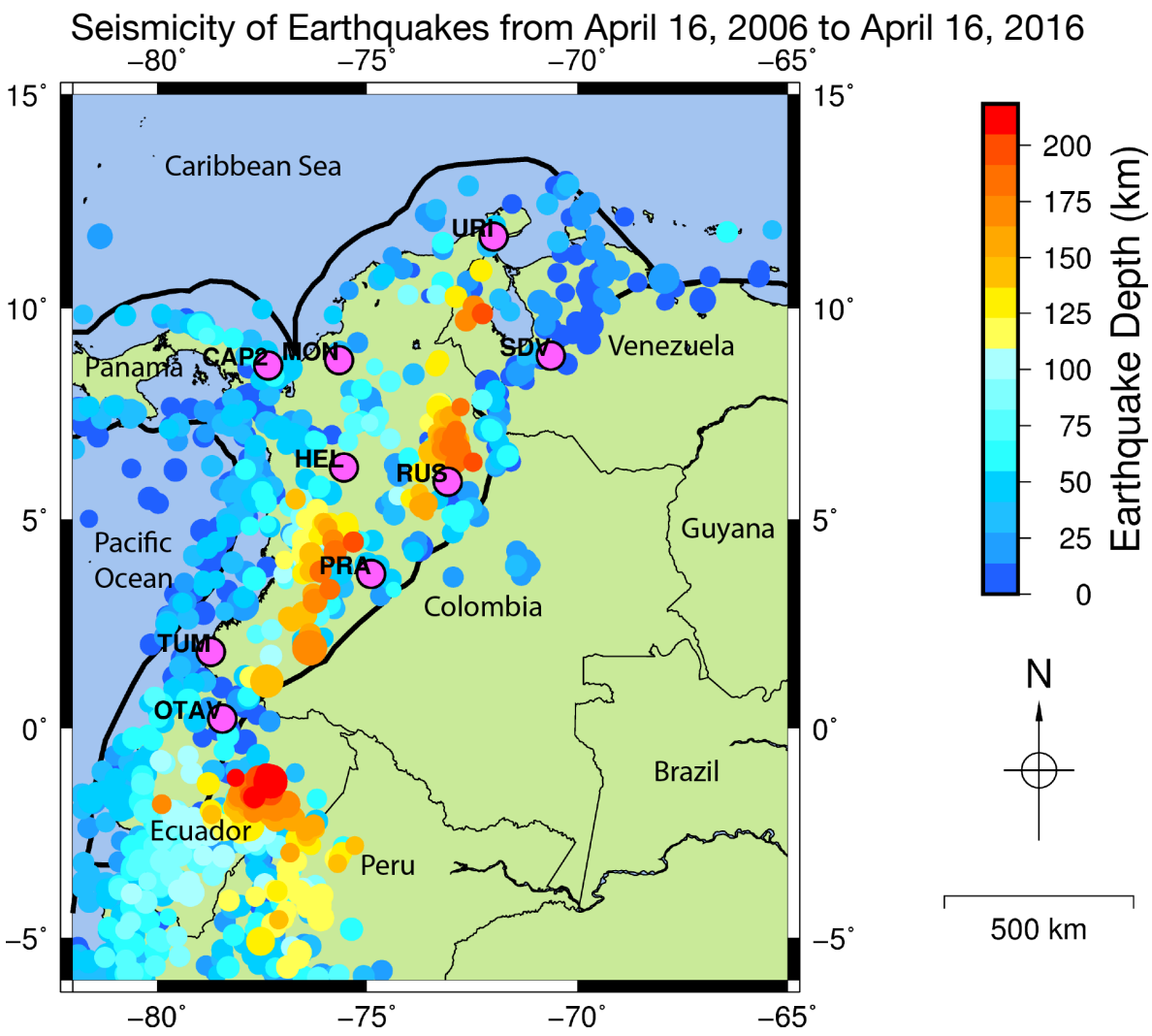

Figure 3: Map of Colombia using historical data from the USGS Earthquake Archives from earthquakes greater than Magnitude 2.5. The magnitudes of earthquakes are sized according to their magnitude and colored according to their depths. The seismic stations used have been marked as purple circles with a black outline. This map uses tectonic boundaries from Bird (2003).

DATA

The data used in receiver functions have been limited to teleseismic earthquakes that occurred between 2012 and June 2015 with a magnitude of 5.6 or greater recorded at stations within Colombia. This data has been downloaded from the Data Management Center at IRIS using the Standing Order of Data (SOD). The data has been downloaded using SOD, with the instrument response removed and rotated to transverse and radial components. The data used in the surface wave dispersion have been limited to surface waves that occurred between 2012 and June 2015 with a magnitude of 4.5 or greater recorded within regional distances of Colombia (catalog provided by IRIS). The earthquakes used used mostly bordered western Latin and South America and the stations used ranged across northwest Colombia (Figure 4).

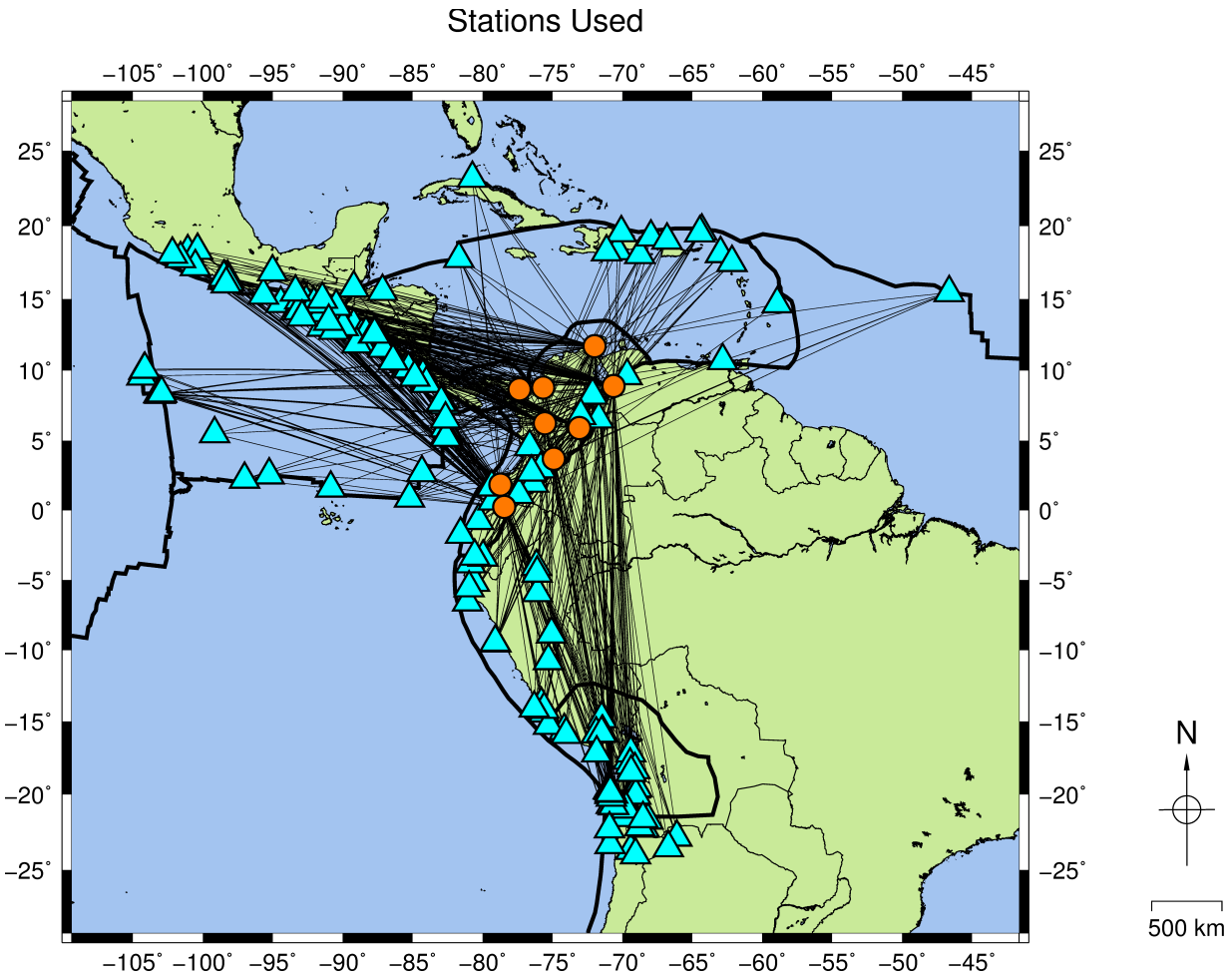

Figure 4: Map of seismic station locations as orange circles and regional earthquake epicenters as blue triangles for the surface wave analysis. Straight paths have been drawn between the earthquake source and the seismic stations. This map uses tectonic boundaries from Bird (2003).

Table 1: Stations used in this experiment to capture data. These stations were deployed across the northwestern portion of Colombia.

Station Latitude	Station Longitude	Station Name
-78.4508	0.2376	OTAV
-70.6340	8.8839	SDV
-75.5477	6.2341	HEL
-74.9013	3.6953	PRA
-73.0830	5.8930	RUS
-71.9900	11.7000	URI
-75.6650	8.7780	MON
-77.3600	8.6500	CAP2
-78.7256	1.8355	TUM
-70.0106	12.5056	AUA1

The program used to calculate the receiver functions, SAC, has been been originally developed by Lawrence Livermore National Laboratory, and has since been maintained by Incorporated Research Institutions for Seismology. The dispersion calculations have been performed using PGSWMFA, a multiple filter analysis code by Charles Ammon (Ammon, n.d.). We use a tomography program, Tomo_sp_cu_s, by M.P. Barmin that had been used in Barmin (2001) to convert our surface wave dispersion measurements into tomography maps. For the joint inversion, we used a primal-dual interior point inversion program created by Anibal Sosa that he used in Sosa at al (2013). Map figures were made using GMT (Wessel, et al., 2013).

Seismic waves carry information about the velocities of the mediums that they pass through, which can be processed to find information about the geology. Two techniques used in geophysics include receiver functions which use P-waves that arrive from deep within the earth and surface wave dispersion which uses Love and Rayleigh surface waves (Stein & Wysession, 2003). Receiver functions do well at resolving discontinuities that show a sharp change in composition but tend to be poor at resolving average velocity structure between structures (Stein & Wysession, 2003). Surface wave dispersion resolves average velocity structure well but tend to be poor at resolving discontinuities (Stein & Wysession, 2003). Their advantages and disadvantages makes these datasets complementary and thus advantageous for use in a joint inversion (Sosa, et al., 2013).

RECEIVER FUNCTION METHODS

Seismic signals represented as digital signals in the time (t) domain show amplitude of seismic energy recorded over time. Signal processing techniques can be performed in the frequency domain for more simple filter calculations. To convert a signal into the frequency (ω) domain, a Fourier transform can be applied to transform a time domain into the frequency domain. Once in the frequency domain, a filter can be easily applied. An inverse Fourier transform can then be applied to transform the resulting frequency domain signal back into the time domain.

Convolution has been defined as a filter that can be equated by the vector multiplication of two signals in the frequency domain, which effectively results in the combination of one signal with another, as seen in Equation 1.

$$C(\omega) = A(\omega) * B(\omega)$$

Equation 1

Deconvolution has been defined as a filter that can be equated by the vector division of two signals in the frequency domain, which effectively results in removing one signal from another, as seen in Equation 2.

$$D(\omega) = \frac{A(\omega)}{B(\omega)}$$

Equation 2

A source-time function has been defined as the shape of body-wave pulses caused by an earthquake rupture (Stein & Wysession, 2003). Earth response has been defined the effects of the Earth's structure (Stein & Wysession, 2003). Instrument response has been defined a function of

a seismometer's response to a frequency and only affects a recorded seismic signal (Stein & Wysession, 2003). A seismograph may be considered the result of convolving the source-time function, the propagation of the signal as a function of the Earth response and the instrument response, as seen in Equation 3. Equation 3 shows the time domain representation of a digital seismograph where $t =$ time, $u(t) =$ seismograph, $s(t) =$ source-time function, $p(t) =$ propogation, $i(t) =$ instrument response.

$$u(t) = s(t) * p(t) * i(t)$$

Equation 3

A three-component seismograph recording typically measures energy on a vertical component measured perpendicular to the surface, and north and south components measured parallel to the surface. The azimuth has been defined as the angular direction from the source and the seismometer. The back azimuth has been defined as the angular direction from which the earthquake signal arrives at a seismometer (Stein & Wysession, 2003). Using a three-component seismograph (a seismogram), the horizontal components can be rotated parallel to the azimuth to calculate the radial component seismograph and perpendicular to the azimuth to calculate the transverse component seismograph (Shearer, 2009). Three dimensional rotation can be achieved by applying a rotation matrix to the signals, as seen in Equation 4 (Jepsen & Kennett, 1990). In equation 4, $\emptyset =$ the back azimuth measured clockwise from north

$$\begin{pmatrix} Vertical \\ Radial \\ Transverse \end{pmatrix} = \begin{pmatrix} 1 & 0 & 0 \\ 0 & \cos\emptyset & \sin\emptyset \\ 0 & -\sin\emptyset & \cos\emptyset \end{pmatrix} \begin{pmatrix} Vertical \\ North \\ East \end{pmatrix}$$

Equation 4

P waves will generate P to S converted phases, named Ps phases (such as Ps, PpPs and PpSs) at interfaces where a change in velocity occurs (Langston & Burdick, 1977). The amount of time in which a Ps wave follows a P wave arrival increases with the depth of the interface at which the Ps wave has been generated (Shearer, 2009). The shape of a Ps wave pulse should be a similar shape as the P wave pulse because Ps signals result from the convolution of the P wave's source-time function modified by the Earth response. A receiver function results from deconvolving the P wave pulse from a seismograph to reveal the Ps phases (Shearer, 2009; Langston & Burdick, 1977). The deconvolution of the two signals from the same earthquake signal results in the removal of the source time function and instrument response (Langston & Burdick, 1977).

Receiver functions map the depth of interfaces between rock layers where velocity changes occur, thus giving a cross sectional view of the Earth. The correlating relationship between P and Ps arrival times and depth allows for a calculated receiver function to be interpolated with seismic velocities assumed from regional rock composition to calculate depth of rock interfaces. An example of using stacking can be seen in Gurrola *et al.* (2015), where stacking seismograms by component from a small distributed array of seismometers and then simultaneously deconvolving the signals can create high quality receiver functions.

Radial receiver functions use the respective components from the energy recorded relative to the teleseismic ray path. The ray path has been defined the path of the propagation of a wave. Teleseismic ray paths have a strong P pulse on the vertical component, strong Ps pulses on the radial component and little P energy arriving on the transverse component, which can be seen in (Shearer, 2009, pp. 90, 200). Radial receiver functions, the most commonly used type of

receiver function to calculate the depths of layers of the Earth's crust, can be calculated by deconvolving the P pulse in the vertical channel with the seismogram from the radial component.

Transverse receiver functions uses the transverse component from the energy recorded relative to the teleseismic ray path. A transverse receiver function will be calculated by deconvolving the transverse component seismogram with the vertical component P pulse. Energy may be recorded on the transverse by conversions due to either seismic anisotropy or dipping structures deflecting P and S waves from the radial and vertical planes (Cassidy, 1992; Langston & Burdick, 1977). The amplitudes and arrival times of transverse energy can be used to detail dipping structures. Ps conversions due to dipping structure can be distinguished from sharp gradients in anisotropy because dipping structure will have a zero delay arrival on the transverse due to the bending of the P wave energy but anisotropic structure will not have a zero delay arrival (Wirth & Long, 2012).

Ps multiples have similar behavior to direct and Ps phases, but have arrival time and amplitude variations affected by back azimuth, dip, interface depth and ray parameters while traveling past a dipping structure (Hayes, 2007). Ps phases results in SV waves which arrive only vertically (Shearer, 2009). Deconvolving the transverse component then should theoretically result in 0 energy on the transverse. Depending on the back azimuth, energy may be recorded on both radial and transverse seismogram components (Cassidy, 1992). The transverse has zero amplitude for arrivals with a back azimuth along the interface's dip direction and the largest amplitude for arrivals traveling along the interface's strike.

Calculating a quality receiver function using signals that pass through dipping stratigraphy can be difficult due to the scattering of energy along dipping structures. With non-dipping stratigraphy, receiver functions calculated with the transverse component as opposed to

the radial component should theoretically be zeroed out due to P and Ps phases occurring only on vertical and radial components. In stratigraphy with dipping structures, Ps converted energy may be recorded on the transverse component due to scattering or erroneous signal behavior (Cassidy, 1992). We propose calculating receiver functions that result from rotating both components along a back azimuth that brings the signal on the transverse receiver function closer to zero amplitude may improve the radial receiver function.

To calculate the receiver functions with minimized transverse energy, we began by rotating the back azimuth of seismographs -15, -10, -5, 0, 5, 10, and 15 degrees from the actual back azimuth to each event. We then calculated both radial and transverse receiver functions by deconvolving their respective horizontal components from the vertical component seismograph. We kept the radial receiver function were the corresponding transverse had lowest corresponding RMS amplitude. We then binned by their ray parameter and stacked to get an average of that bin.

RECEIVER FUNCTION RESULTS

RMS amplitude may be used to make comparisons of amplitude between signals. RMS amplitude has been calculated using the square-root of the mean of the square of all amplitude values. The RMS amplitude has been used to compare the energy on each component for each of these receiver functions. In the receiver function figures, the receiver functions have been labelled on the right side with their station name, whether they have been calculated on the radial or transverse and labelled “R” and “T” respectively, and with the date and time of the event.

We calculated a test to confirm the concept that rotating the data would lower the transverse energy. The seismic wave in this example had been captured by station PRA that has been deployed near the North Andes - South America plate boundary. At +10 degrees back azimuth rotation, the transverse had the lowest RMS amplitude, much lower than the non-rotated version (Figure 6). At +15 and +5 degrees, the RMS amplitude of the transverse decreased where the +5 measures slightly lower. This implies that there should be an optimal angle in the range from +5 to +10 that could be used to lower the transverse amplitude. decreases the overall RMS amplitude going more negative towards -15. The radial receiver function at the +10 degrees has a nearly negligible increase in amplitude compared to the non-rotated 0-degree receiver function and the overall shape did not change much.

By rotating the seismographs, the radial receiver functions tended to grow in RMS amplitude where transverse receiver functions decreased in amplitude or stayed the close to the original value. This may be a function of conserving energy in the system where the energy from the transverse has been oriented in a more radial direction.

Reorienting the back azimuth to lower the amplitude of energy in the transverse may be accomplished by aligning the back azimuth along the direction of the dipping structure.

Calculating receiver functions that result from rotating both components to bring a transverse receiver function closer to the zero has little difference to the radial receiver function.

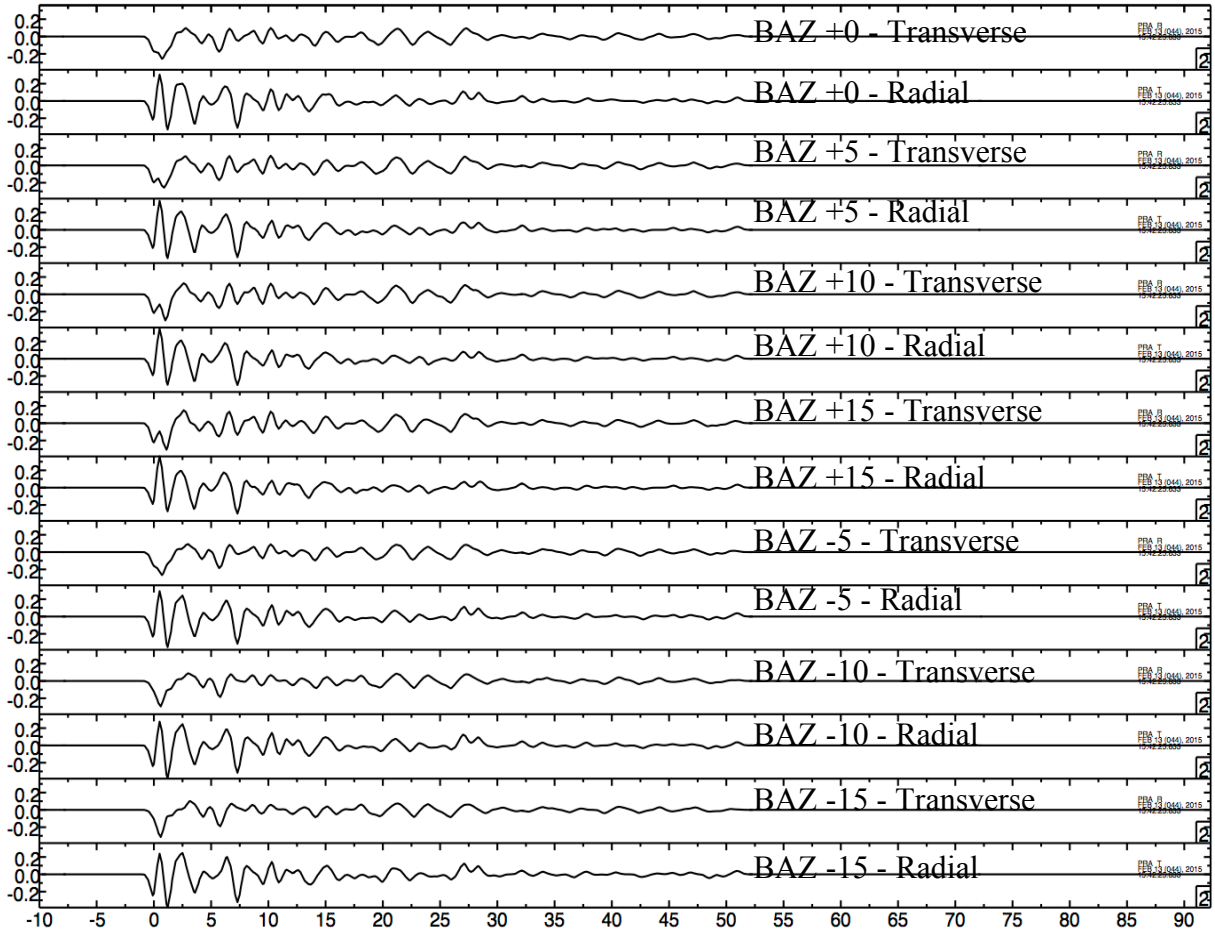

Figure 5: Rotated receiver functions using data from station PRA using the signal from an earthquake which had a 60.2 degree GCARC and a 28.2 degree back azimuth from the station.

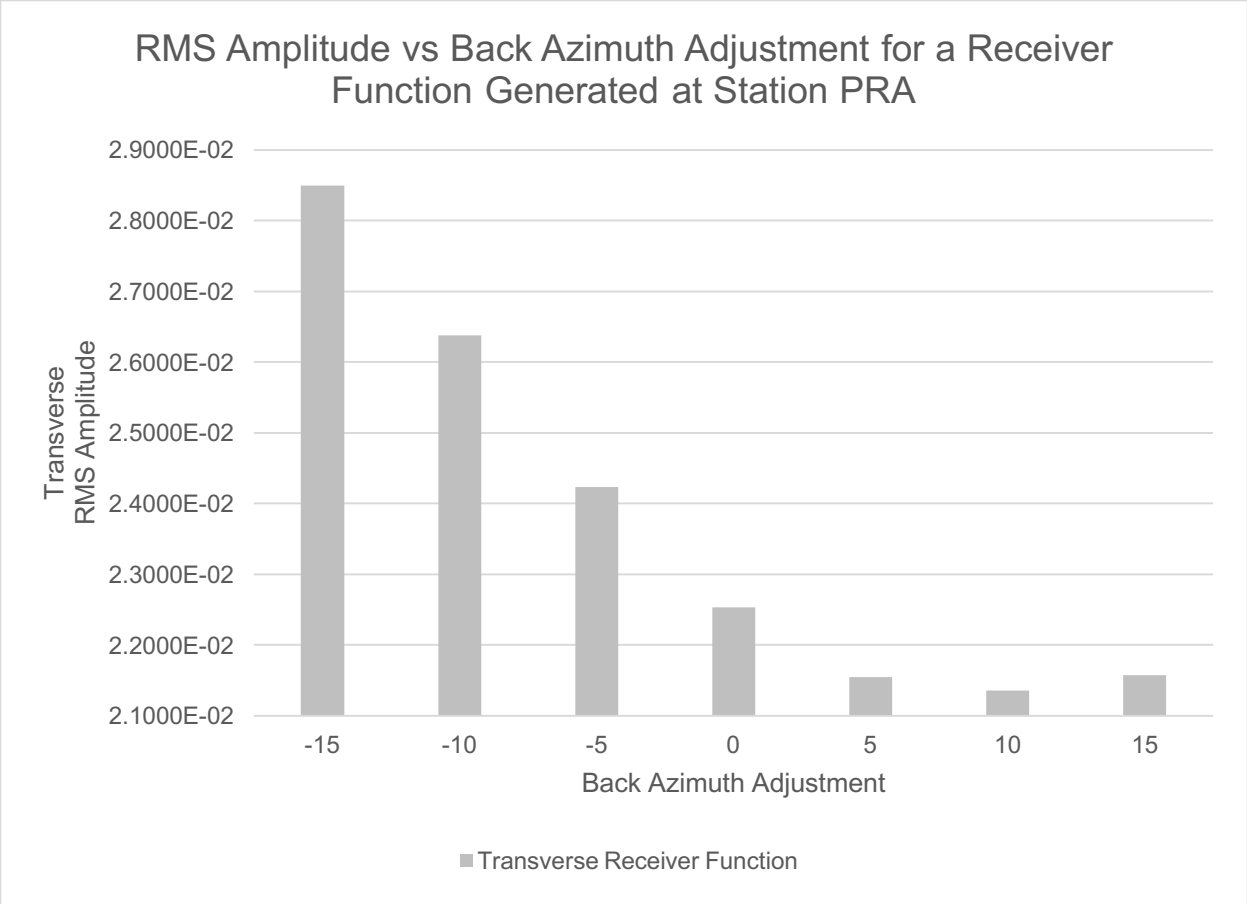

Figure 6: The calculated RMS rotated transverse receiver functions calculated at incremental back azimuths from -15 to +15 from station PRA

SURFACE WAVE DISPERSION METHODS

In an earthquake, surface waves will be low frequency, high amplitude waves that follow the P and S body waves (Sosa, et al., 2014; Sosa, et al., 2013; Shearer, 2009; Stein & Wysession, 2003). Surface waves vary in velocity as a function of depth as sampled by a period resulting in dispersion which allows for the study of the Earth's velocity structure (Stein & Wysession, 2003; Shearer, 2009). Lower frequencies (higher periods) travel deeper within the earth (Stein & Wysession, 2003). Love wave dispersion depends on shear velocity and Rayleigh waves depend on both compressional and shear velocities (Stein & Wysession, 2003).

The advantage of calculating surface wave dispersion would be its superior ability to resolve average velocity structure as a function of depth. For surface wave dispersion, we take use an inversion process called surface wave tomography to create 2-D dispersion maps of velocities using a process. A surface wave dispersion curve compares group velocity against the period calculated at a location. The group velocity has been defined the slope of the wave (Stein & Wysession, 2003). Instead of processing each event individually, we calculated the dispersion automatically using PGSWMFA.

For the set of surface waves, a large variation had been found in the quality of the surface waves measurements so we ran processing to remove unstable group velocities. We began by removing measurements from the raw period versus group velocity curves that did not have periods higher than 55 seconds because higher periods would be needed to see deeper into the earth. We then separated Love waves from the Rayleigh waves. If the Rayleigh did not have a vertical channel, we kept the radial channel.

For each surface wave type, we used constraints to further remove bad data and create a separate dataset for processing. We calculated the surface wave measurements into surface wave

dispersion curves that measure period versus group velocity. We calculated our surface waves up to 150 seconds period. We initially removed the first periods of 20 seconds or less to reduce noise. We took the average of the of the group velocity for each period and the compared that average to the period of each signal using a standard deviation of 0.6. We chose a standard deviation of 0.6 after trying many standard deviations and compared the results. When tested against the average, if the group velocity fell outside standard deviation, it and threw the rest of the periods out and then calculated a new overall average.

Once we completed the standard deviation test, we tested to ensure a stable rate of change for group velocities. Where the rate of change increased or decreased too sharply, we tossed out the rest of the periods of that surface wave. These tests resulted in 1058 surface wave measurements being used from the original data set; 327 Love waves (Figure 7) and 731 Rayleigh waves (Figure 8).

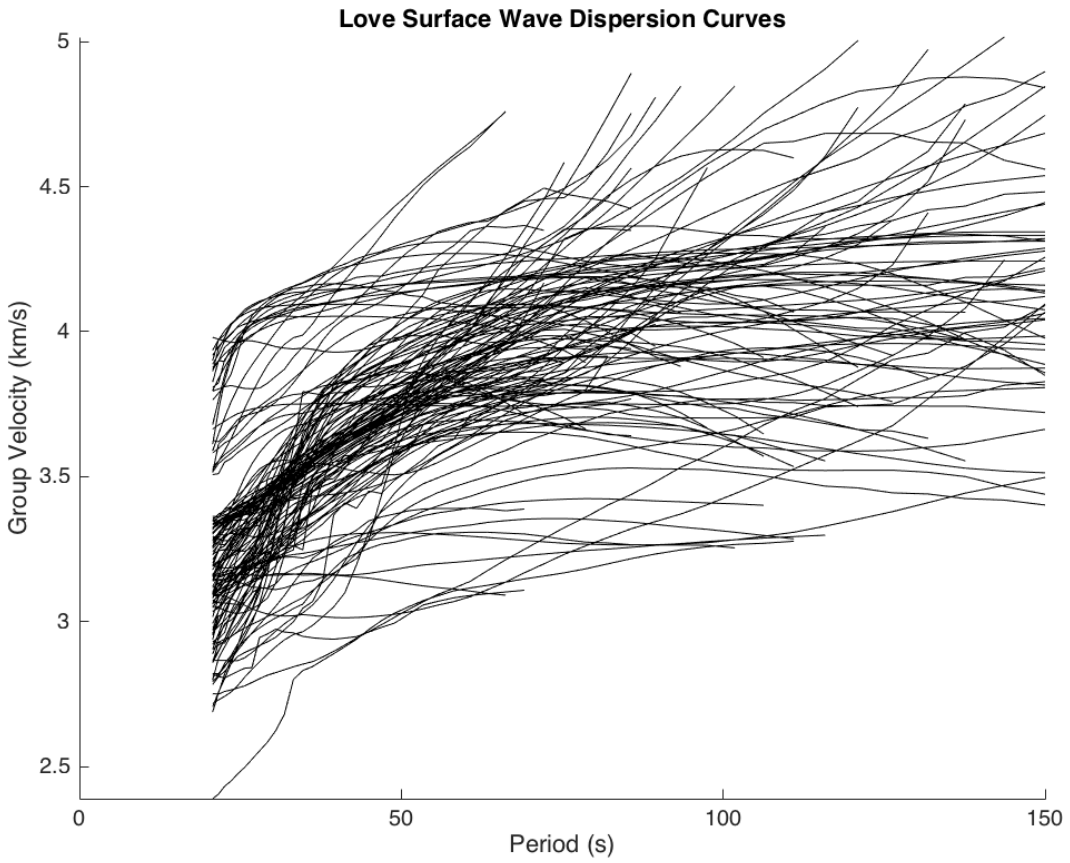

Figure 7: Love Surface wave dispersion curves filtered after filtering out too short, data that fell outside of a standard deviation of the average. Higher periods correspond to a higher depth in the earth. These data will next be used in the Love set of tomography to make a map of velocities.

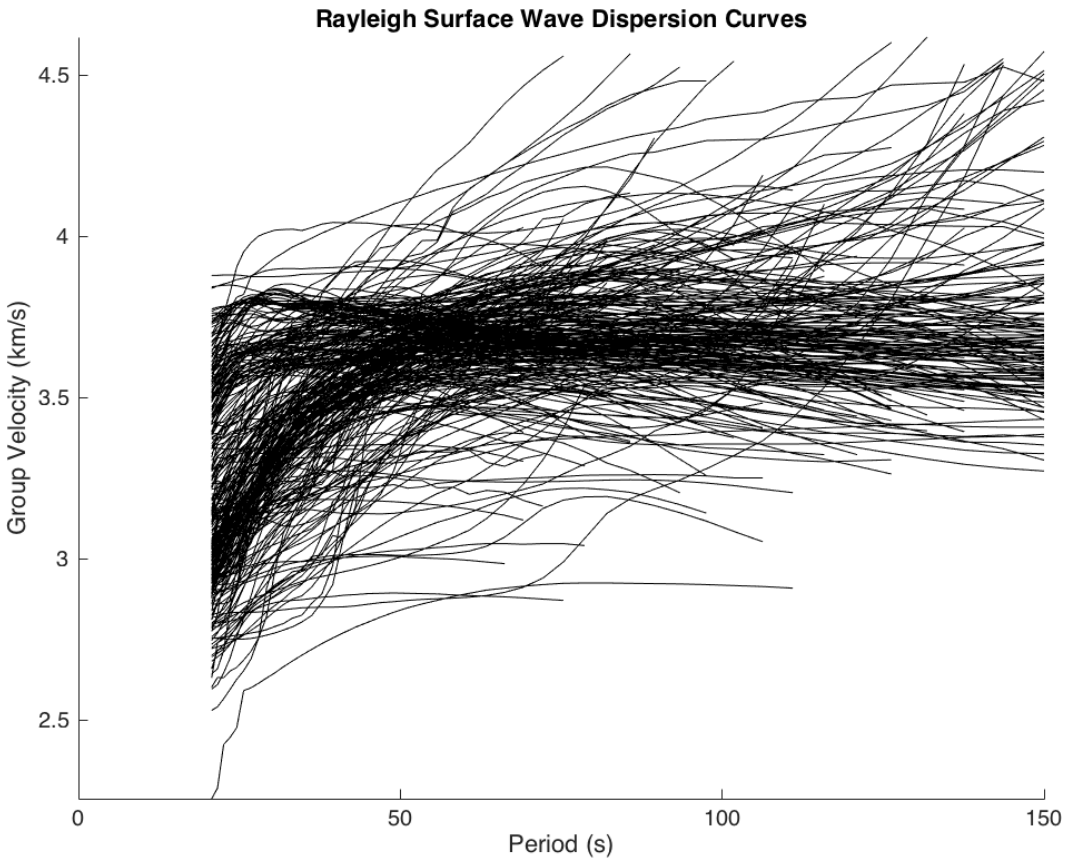

Figure 8: Rayleigh Surface wave dispersion curves filtered after filtering out too short, data that fell outside of a standard deviation of the average. These data will next be used in the Love set of tomography to make a map of velocities. Higher periods correspond to a higher depth in the earth. The quality control resulted in many more curves in the Rayleigh set than the Love set.

SURFACE WAVE DISPERSION TOMOGRAPHY

After we quality controlled the curves, we used them in a Gaussian beams method tomography to calculate the regional surface wave group velocity measurements for each period. This tomography results in a 2-D map of velocities. The Gaussian tomography method treats surface waves as rays sampling an infinitesimal zone along the great circle arc between the source and receiver and interpolates based on the three nearest neighbors (M. P. Barmin, 2001). The tomography ignores scattering that we may find (M. P. Barmin, 2001). The program applies constraints including Gaussian smoothing and amplitude ranges (M. P. Barmin, 2001). The tomography used a 1-D PREM model to predict the travel time for waves.

For the surface wave dispersion tomography inversion, it took some trial an error of tweaking the smoothing damping coefficient and the Gaussian for smoothing to get a quality looking tomography map. This allowed for stable tomography that was not oversmoothed. We generated new period versus group velocity curves using the location of each seismic station from the calculated tomography maps with the corresponding wave type (Figure 13).

In the program there are settings to adjust the Gaussian and damping coefficient. We ran multiple combinations trying different increments of the values. We pursued values that did not overdamp the maps and had curves that increased smoothly. We lowered the damping values until they the maps had high velocity and low velocity areas that resembled the boundaries of the tectonic plates. We arrived at using smoothing damping coefficient of 400 and a 300km Gaussian for smoothing.

As we increase periods, we note the trend of an overall increase in velocity that would be of the Nazca boundary follows the shape of the Panama plate and the South America plate boundary. At higher periods, that high velocity can be seen in central Colombia. At the Caribbean – North Andes boundary, at periods above 80s, we see a rise in velocity where we expect the Caribbean plate to be subducting. From 34 to 39s, we see a low velocity that continues underneath the southwest portion of the North Andes plate. This could be from the South America plate subducting beneath the North Andes plate. From 85s and above, a high velocity zone that runs from north to south may be a slab from the Nazca plate due to it being parallel with the boundary.

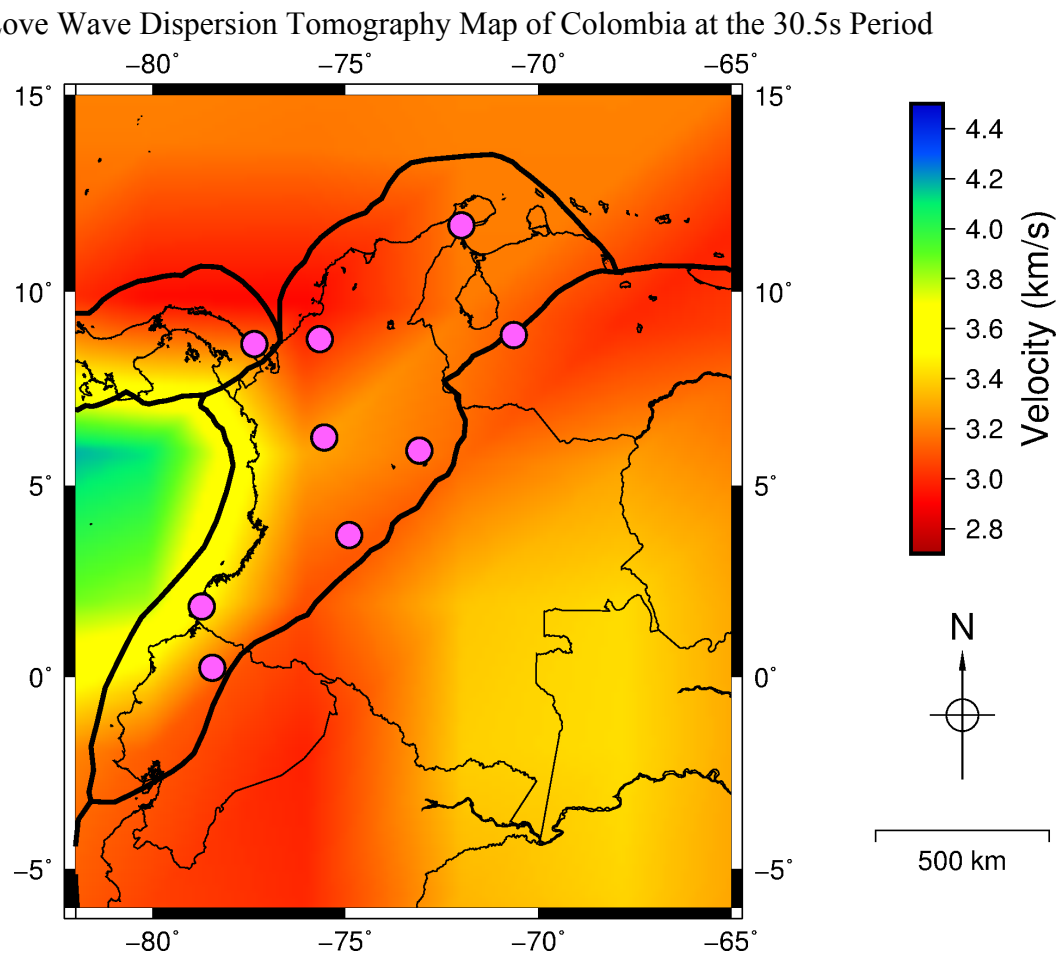

Figure 9: Map of a final Love Surface wave dispersion map that had been calculated at 30.5s period. The purple circles on the map corresponds to seismic stations. This map uses boundaries from Bird (2003).

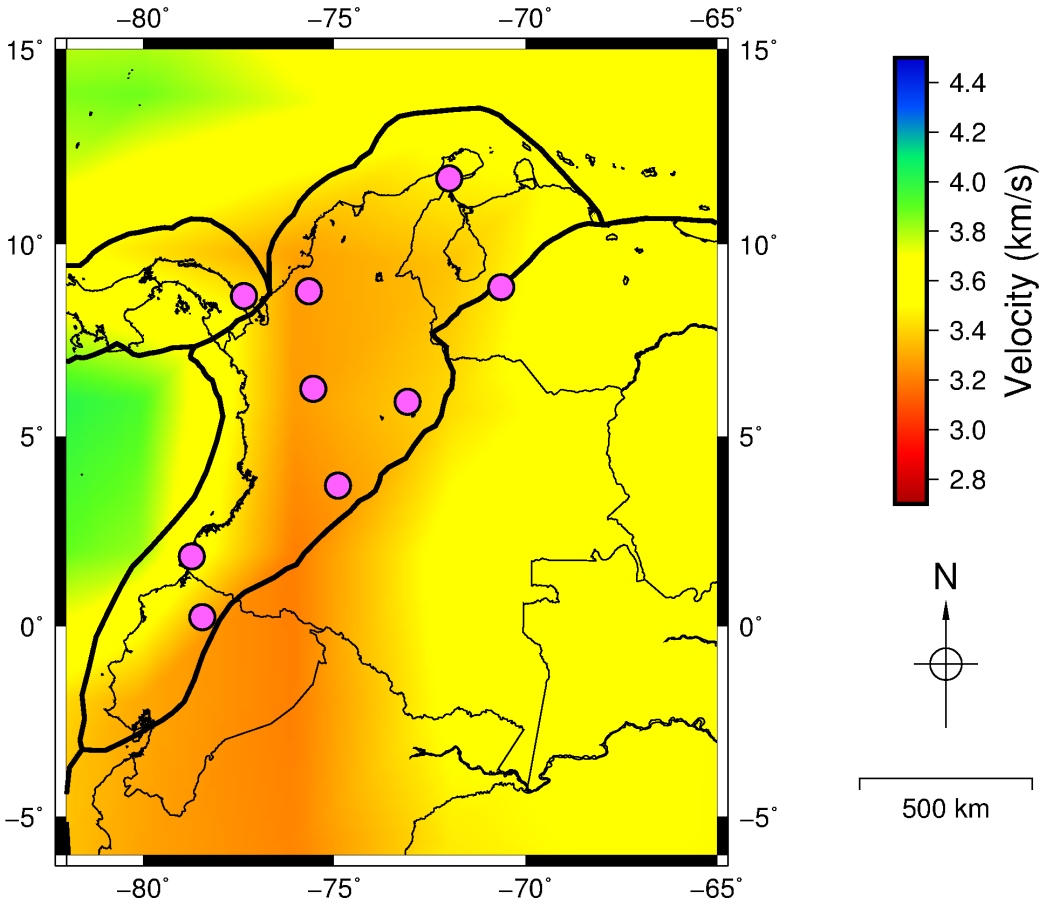

Figure 10: Map of a final Love Surface wave dispersion map that had been calculated at 39.49s period. The purple circles on the map corresponds to seismic stations. This map uses boundaries from Bird (2003).

Raleigh Wave Dispersion Tomography Map of Colombia at the 85.71s Period

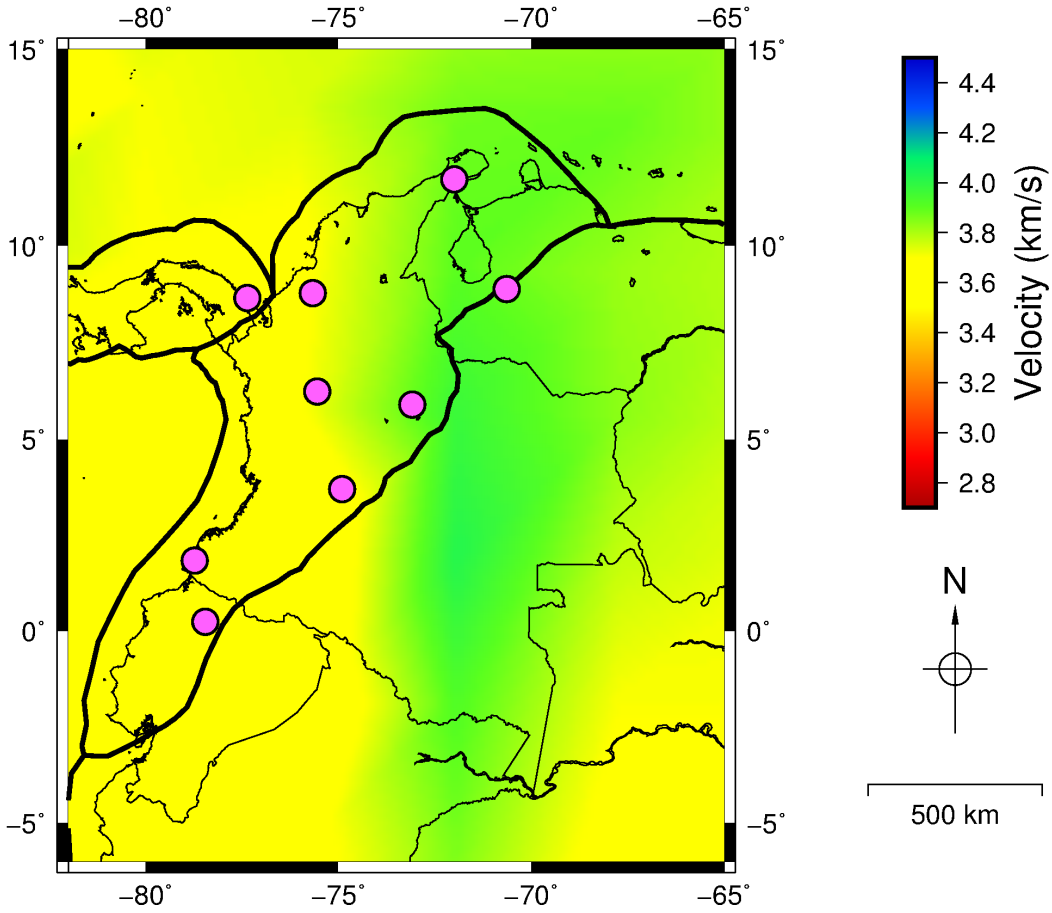

Figure 11: Map of a final Raleigh Surface wave dispersion map that had been calculated at 85.71s period. The purple circles on the map corresponds to seismic stations. This map uses boundaries from Bird (2003).

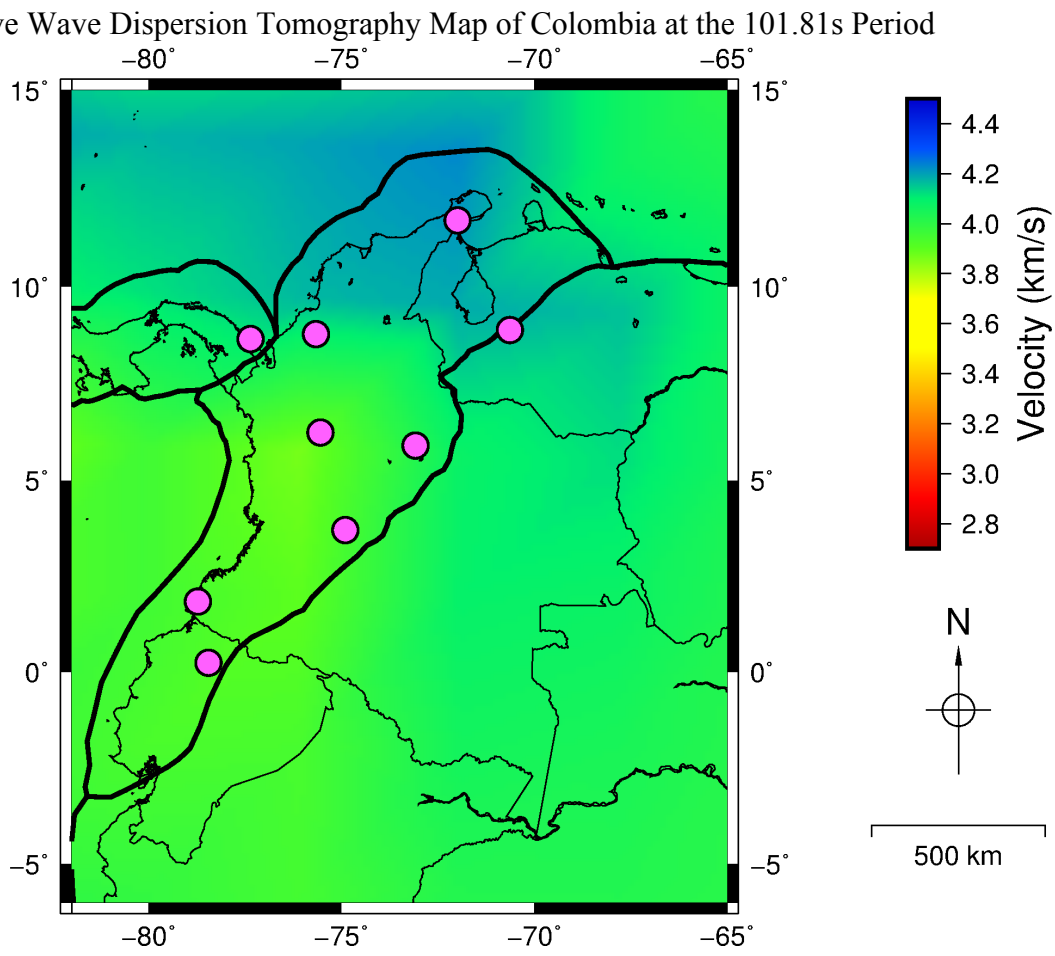

Figure 12: Map of a final Love Surface wave dispersion map that had been calculated at 101.81s period. The purple circles on the map corresponds to seismic stations. This map uses boundaries from Bird (2003).

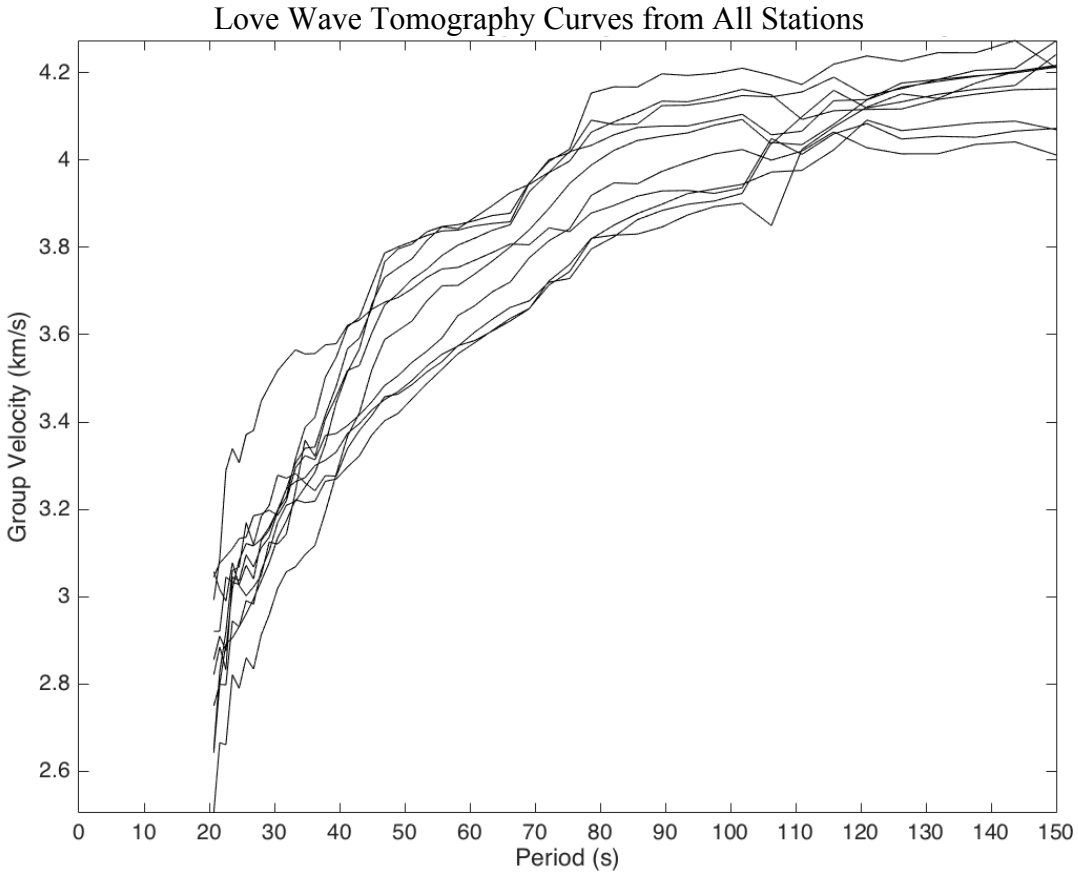

Figure 13: Using each seismic station's longitude and latitude, we used the group velocity at that point from each period of the tomography map. We can see a general increasing trend of group velocity with the period. This surface wave dispersion curve has been made using the tomography maps made from Love waves.

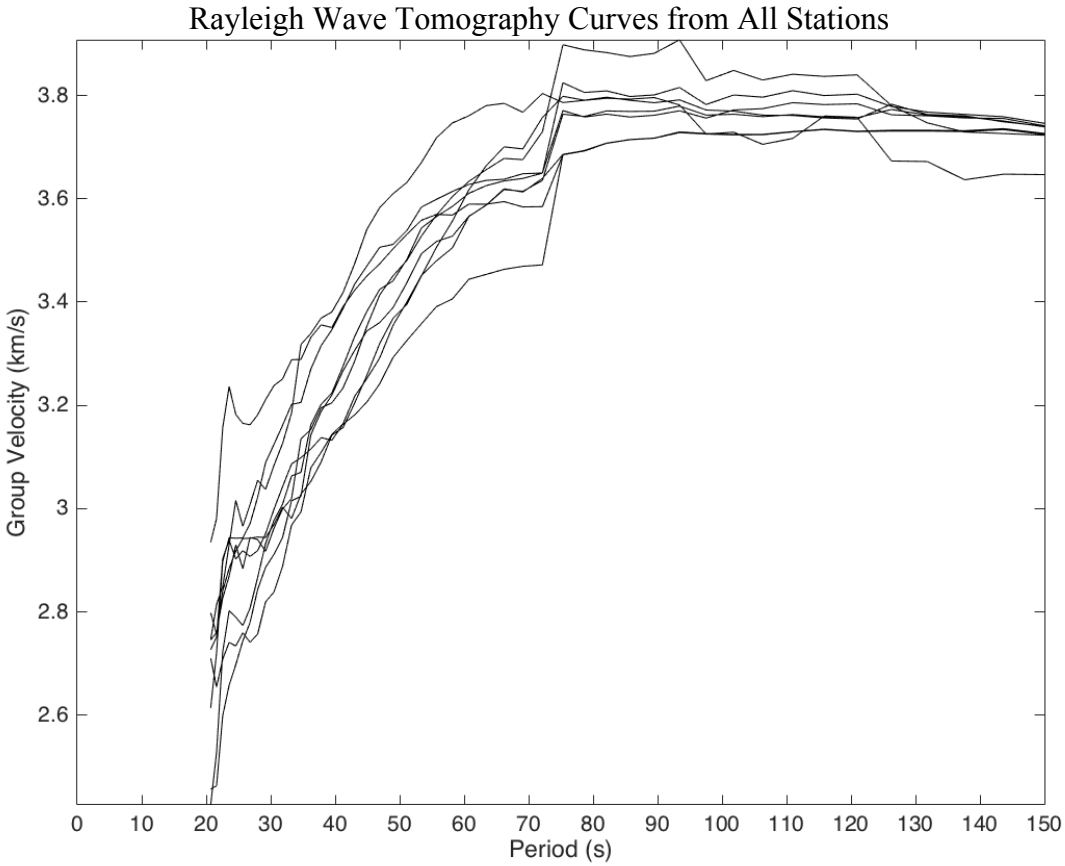

Figure 14: Using each seismic station's longitude and latitude, we used the group velocity at that point from each period of the tomography map. We can see a general increasing trend of group velocity with the period. This surface wave dispersion curve has been made using the tomography maps made from Rayleigh waves.

JOINT INVERSION METHODS AND RESULTS

Joint inversion can generate improved models using data sets that may have different sensitivities and resolutions (Sosa et al. 2013). We will generate a model using both our receiver functions and surface wave dispersion models because because theoretically the datasets should be consistent and complimentary (Julia, et al., 2000). A system will be consistent if the data set samples the same propagating medium, and complementary if the resolution of the inverted model increases which we attempted to do (Julia, et al., 2000).

We adopted a joint inversion method that has seen success with the combination of receiver function and surface wave dispersion data from the joint inversion least-squares (LSQ) algorithm as seen in Sosa et al. (2013) which he named “primal-dual interior point inversion” or PDIP for short. PDIP has shown improved computation speed and reduced noise over another previous method, truncated singular value decomposition, due to the addition of explicit inequality constraints as a priori information (Sosa et al. 2013). Dr. Anibal Sosa performed the joint inversions in this research by computing joint inversions using our surface wave dispersion and with our receiver functions that had been calculated with minimized transverse components.

DISCUSSION

From analyzing the seismicity in the region in relation to the seismic station locations, the Nazca plate subducting at 25 to 50 km depth (Figure 3) below the stations OTAV and TUM. The station PRA should be above subducting south American slab and a collision with a slab from the Nazca plate. The RUS station should be above the collision of the two slabs as described in Zarifi et al. (2007) as well as the horizontal subduction of the South America plate beneath the North Andes microplate. Station SDV will be directly on the border of the South American - North Andes boundary. HEL appears to be in a spot that will likely only measure the North Andes microplate. The stations AUA1, URI and MON should be above the Caribbean subduction at 25 to 50 km depth. CAP2 is on the border of the North Andes microplate and and the Panama microplate.

The joint inversion calculates shear velocity as a function of depth. A model of expected velocities for these depths has been overlaid for a comparison. Each station has a joint inversion calculated so that we may analyze the presence of slabs at the depths below. We compared our joint inversion models with the 1-D PREM velocity model. We identified crust slabs at depths where a low velocity, which could be a mantle wedge, has been followed by a high velocity which would be a slab.

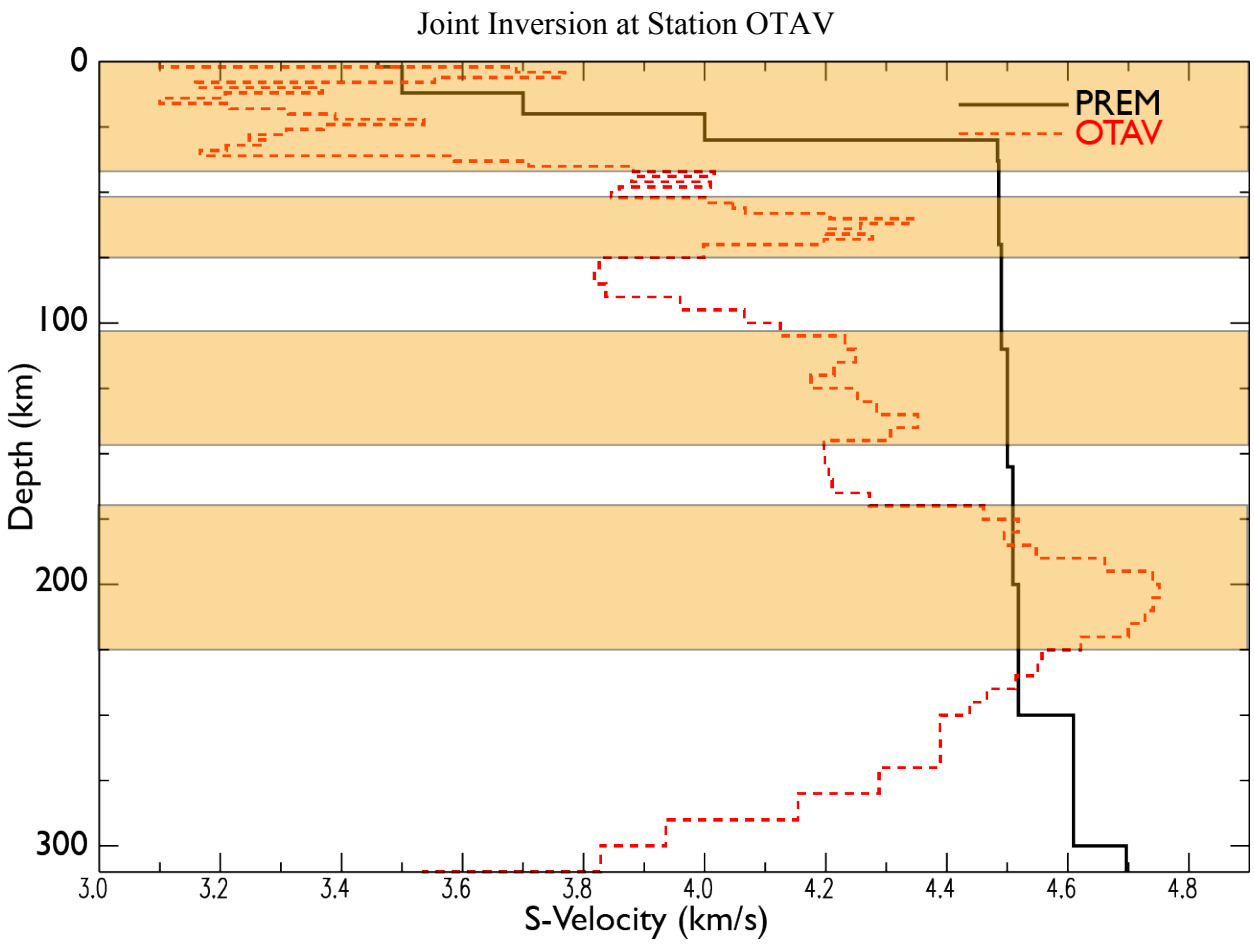

Figure 15: The joint inversion model at station OTAV

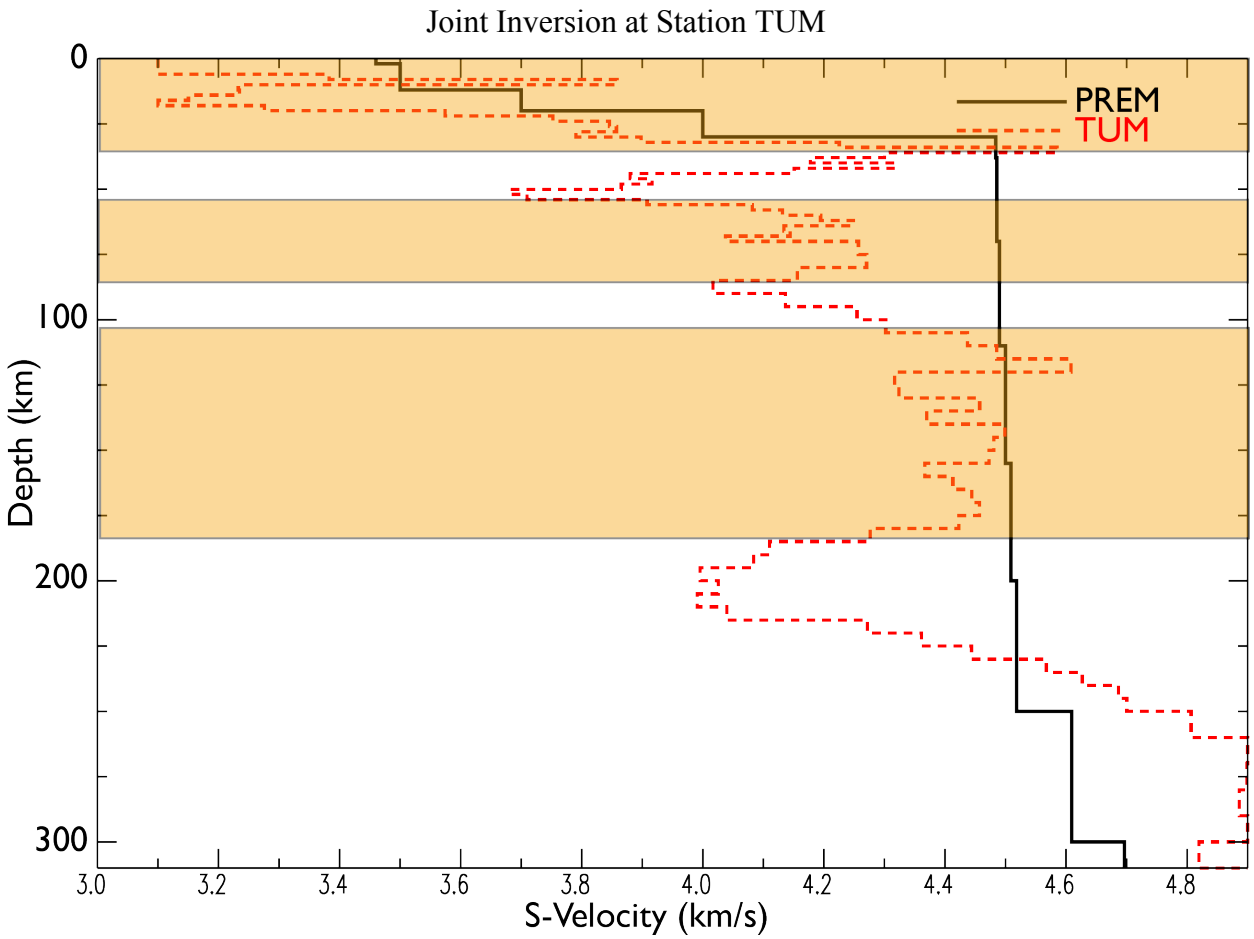

Figure 16: The joint inversion model at station TUM

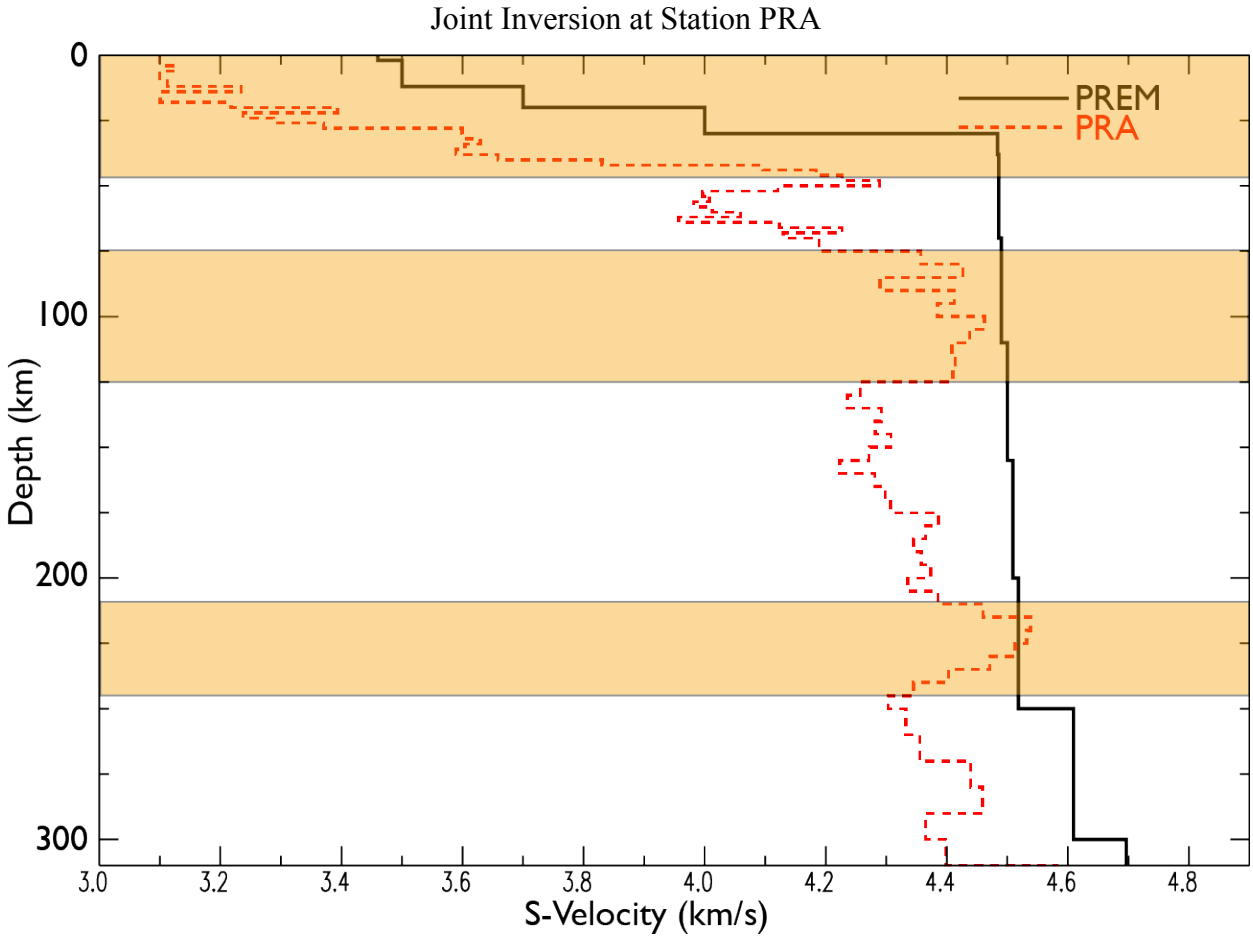

Figure 17: The joint inversion model at station PRA

The furthest south on the North Andes – South America plate boundary, OTAV, has a crust of about 60 km thick. The crust appears to be 40 km thick below this area. From 50 to 75 km depth, we see what would likely be the Nazca plate. From 110 to 145 km there is a velocity low that culminates in a return to the deepest crust velocity for about 40 km. This may be more of the broken slab seen in TUM. From 180 to 215 km, we see what may be a slab that would likely also have come from the Nazca Plate.

At TUM, the crust appears to end at 35 km depth. From 55 to 80 km, there is an increase in velocity indicating the presence of the subducting Nazca plate. From 110 to 180 km depth, there is an increase in velocity indicating the presence of a deep detached slab from the Nazca plate with the plate at a steep angle This follows the other station on the boundary, OTAV, which begins increasing at about this depth which asserts my suspicion that this is the depth of the Nazca plate in this area. 215 km to 400km there is a dramatic velocity high above what we may expect from the mantle. This could indicate crust from the Nazca subduction that broke off and is now lying at the boundary of the upper mantle and may be related to the deep increase of velocity seen just south beneath OTAV.

Curiously, PRA appears to end its crust at about 45 km in depth continuing the pattern. From 75 to 125 km, we see a continuation of the Nazca slab a bit deeper in the mantle. From 215 to 245 km, see a slab that could be the eastern portion of the Caldas tear.

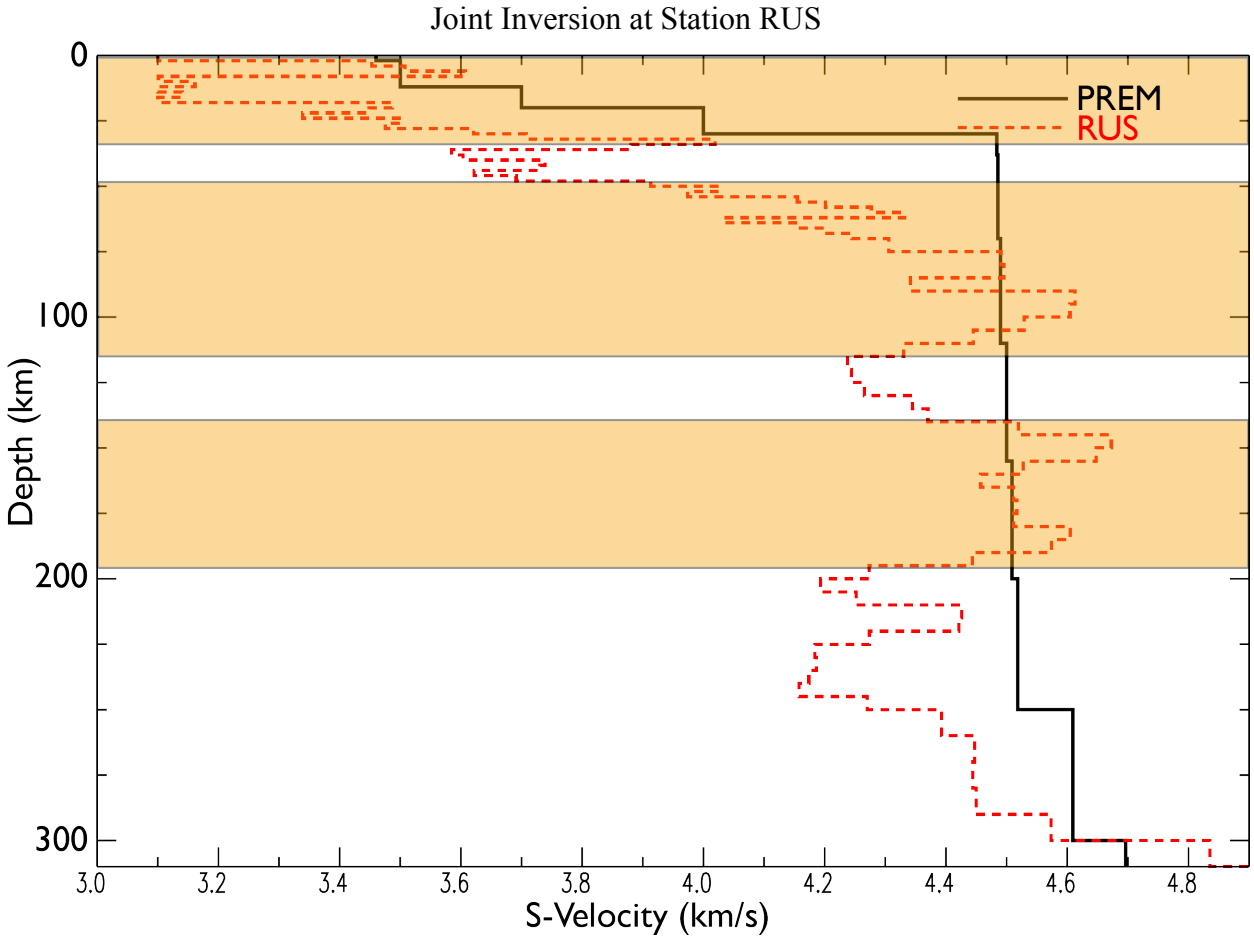

Figure 18: The joint inversion model at station RUS

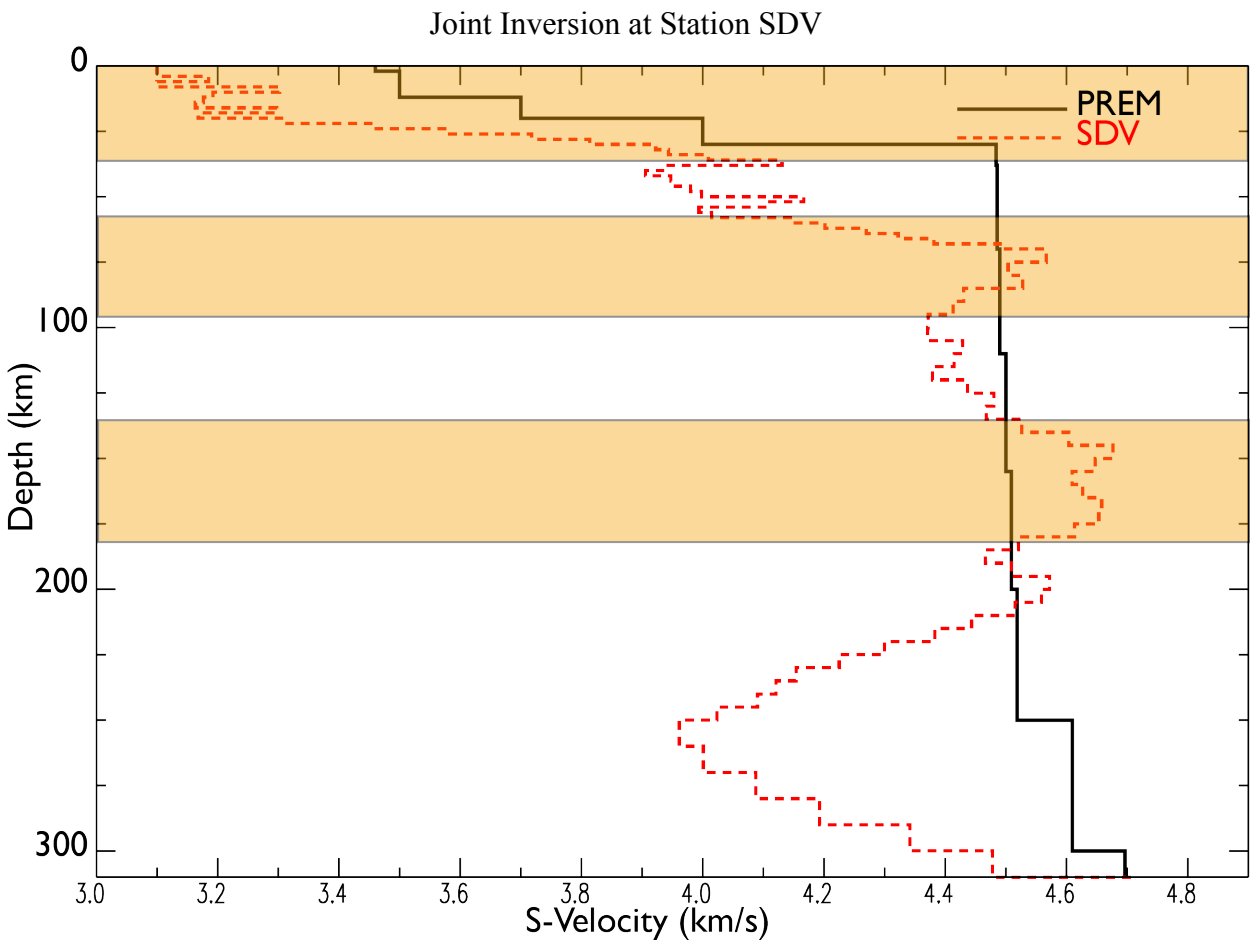

Figure 19: The joint inversion model at station SDV

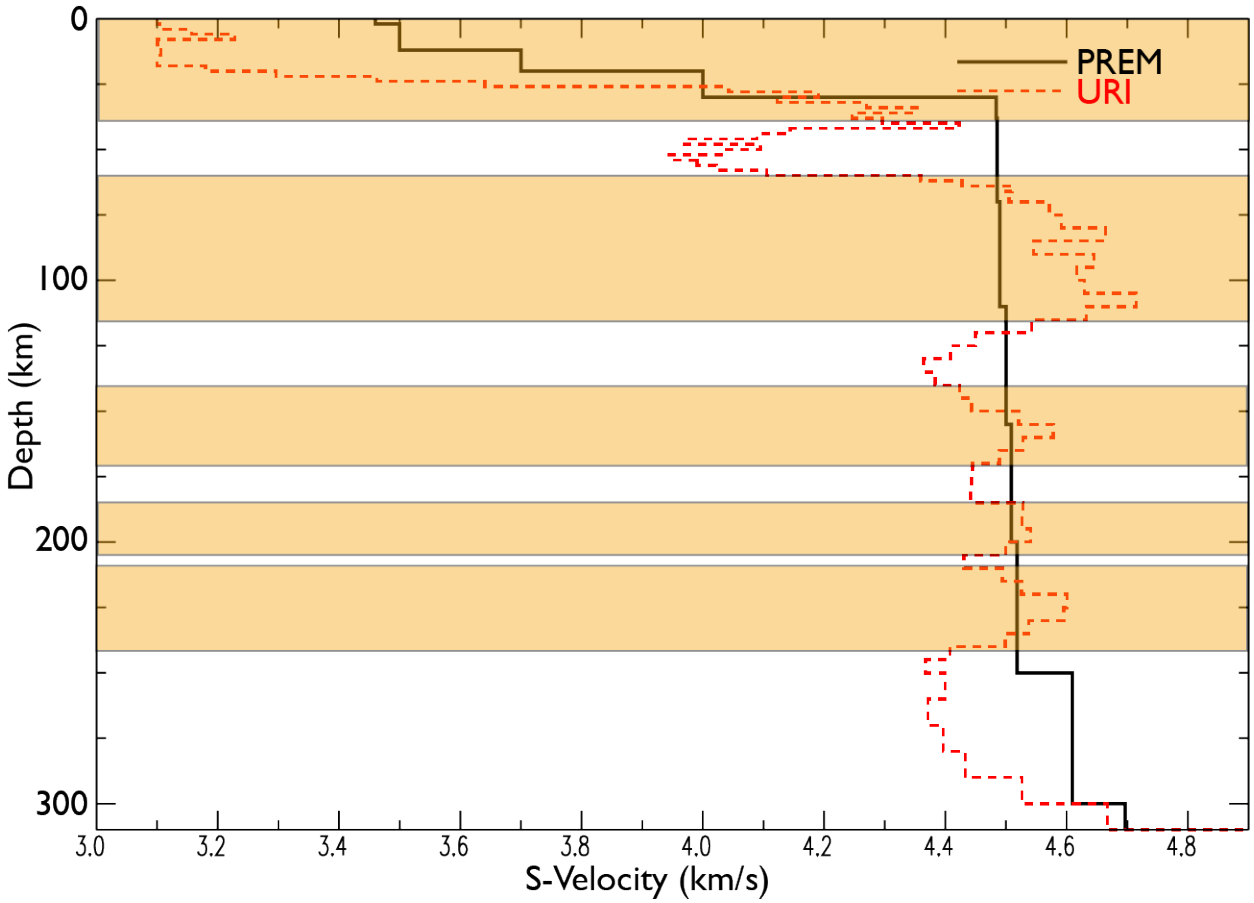

Figure 20: The joint inversion model at station URI

We expected station RUS to above the collision of the two slabs as described in Zarifi et al. (2007) as well as the horizontal subduction of the South America plate beneath the North Andes microplate. The crust here ends at about 35 km. At depths from 50 to 115km, this could be the South America slab subducting just beneath the crust as expected. This may be due to the delamination of the South America plate. At 135 km to 190 km depth, we see the southern of the two slabs that cause the seismicity of the Bucaramanga Nest (Zarifi, et al., 2006). This could be one of the two slabs that cause the seismicity of the Bucaramanga Nest.

The station SDV, directly on the border of the South American - North Andes boundary near the transform boundary of the Caribbean plate, shows a similar crust depths of 35 km. From 60 km to 90 km, we see a continuation of the South America plate subducting less than 25km from the crust. From 135 to 180 km depth, the 0.2 km/s increase compared to the mantle may be a portion of slab that is still breaking apart. Below this point is a 0.4 km/s difference in expected velocities. This behavior is replicated in stations OTAV, PRA, RUS and SDV nearest the North Andes – South America plate boundary but not in other stations except below MON at the Caribbean – North Andes boundary.

For the most part, URI follows the model particularly well, especially where the crust ending at about 35 km deep and in the upper mantle. From 60 to 115 km, we believe there lay the South America plate as we haves seen across the boundary. 125 km is where we estimated the start of the the Caribbean plate but we also see a plate at 185 km. This is hard to determine which plate may be which.

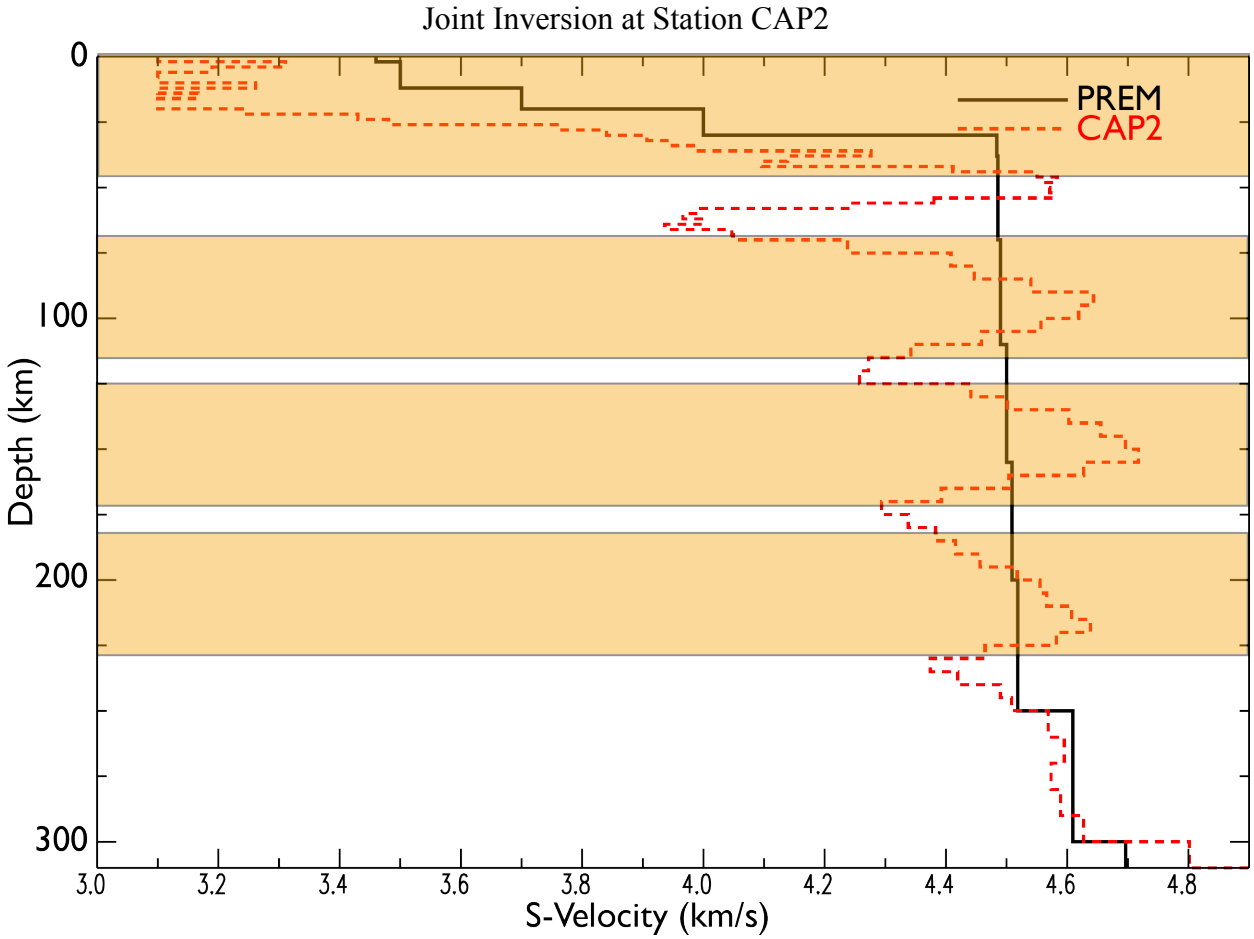

Figure 21: The joint inversion model at station CAP2

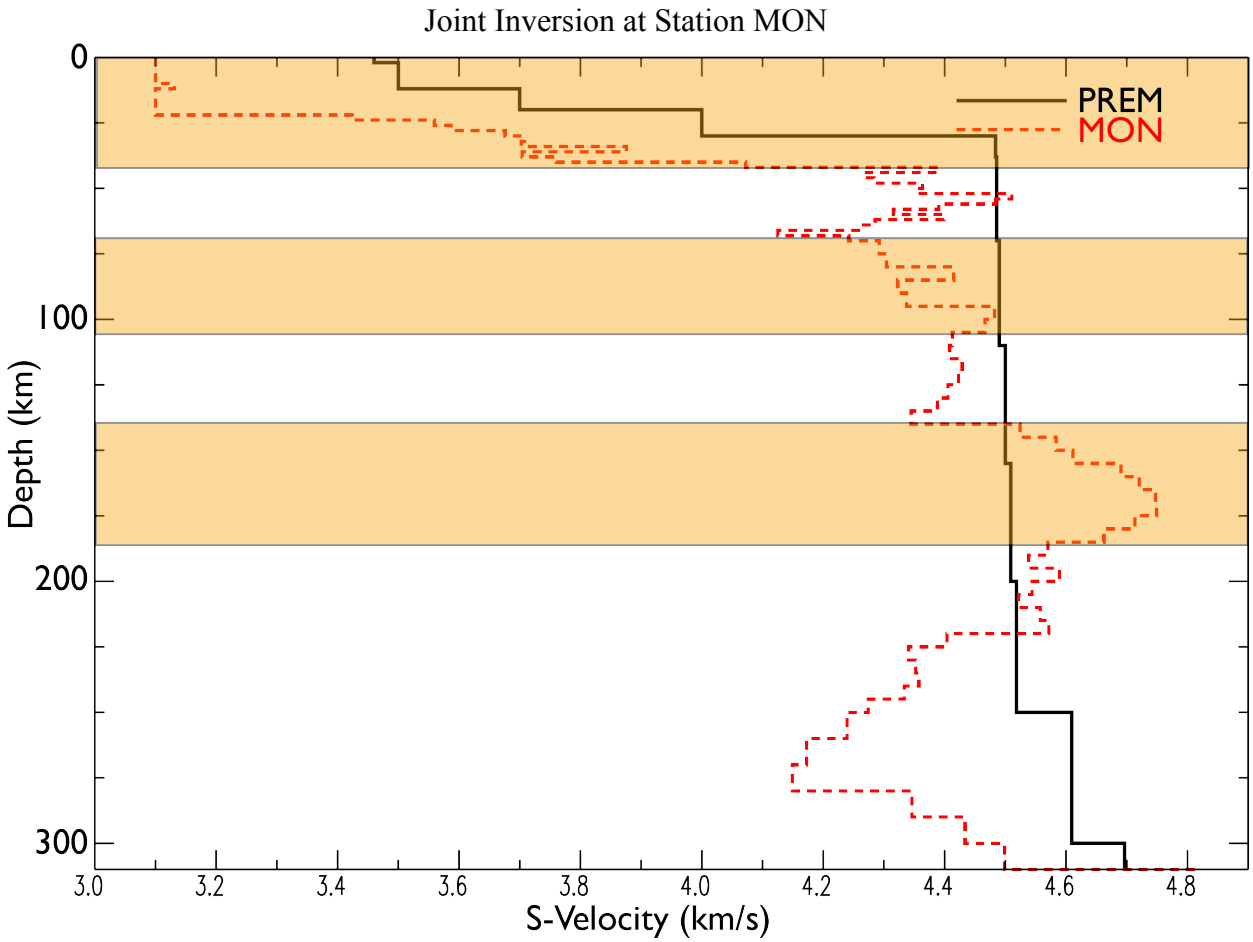

Figure 22: The joint inversion model at station MON

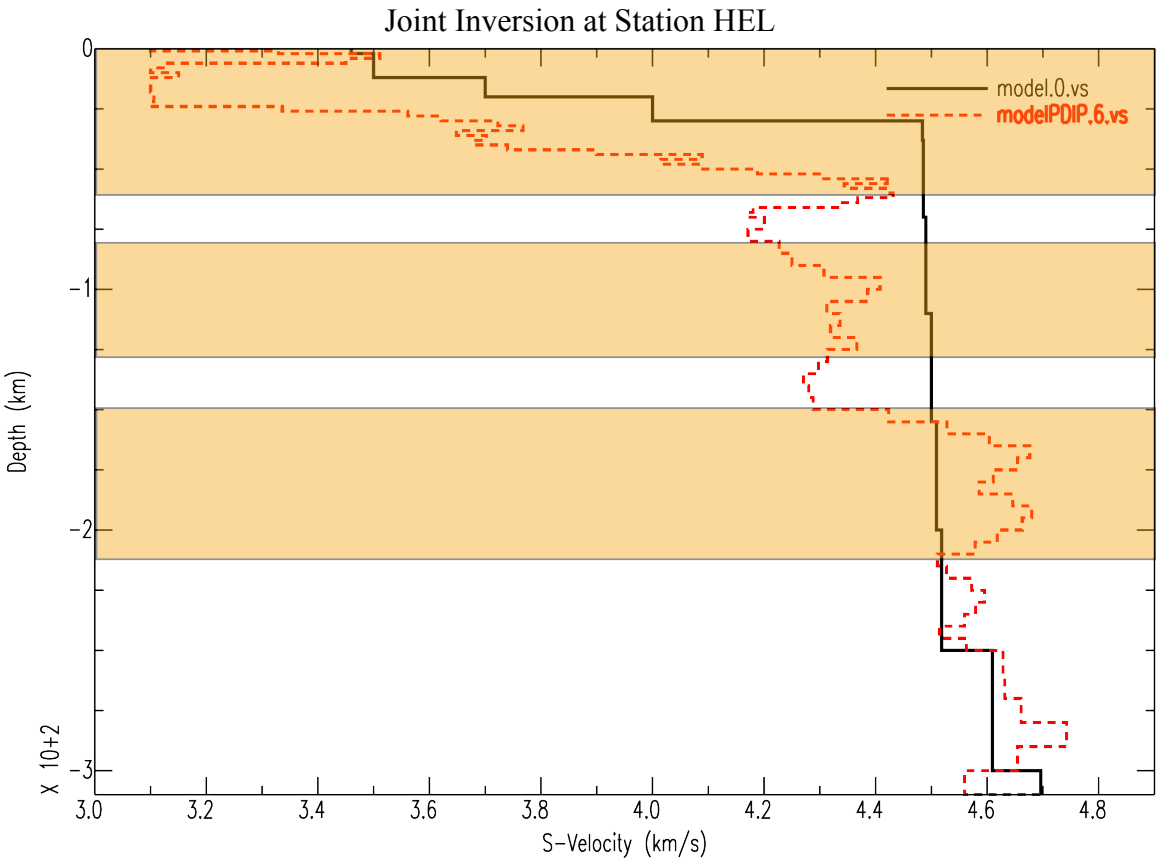

Figure 23: The joint inversion model at station HEL

On the southern border of the North Andes microplate and and the Panama microplate, CAP2 would hopefully be able to shed some light on its behavior. The calculated crust model fits the expected values well but then shows a series of velocity highs and lows going down into the mantle. From 65 to 115 km, the velocities indicate the presence of a slab. This may be a continuation of the South America plate as seen below station URI. Starting at 125 km, a velocity high which doesn't match that of the nearby station MON which we believed to be the Caribbean plate. At 250 km and below, the model fits well so there may be something to this pattern. CAP2 is located between the Panama, Caribbean and Nazca plate so the behaviors of these plates may have left crust beneath the area. Perhaps a series of plates the had been periodically torn off and sunk into the mantle like cards.

The crust below MON ends at about 35 km. Curiously, at 135 km depth, we believe we see the Caribbean plate. The calculated crust model fits the expected values well but then shows a series of velocity highs and lows going down into the mantle. From 70 to 110 km, the velocities indicate the presence of a slab. This may be a continuation of the South America plate. Starting at 125 km, this puts this depth appropriate for the Nazca or Caribbean plate. CAP2 is located between the Panama, Caribbean and Nazca plate so the behaviors of these plates may have left crust beneath the area. Underneath the Panama microplate, there has surely been a collision of the Nazca and Caribbean plates. Perhaps these series of plates the had been periodically torn off and sunk into the mantle like cards.

In the center of Colombia, below HEL, the crust has an absurd 60 km thickness comparable to those along the North Andes – South America plate boundary. This could be due to bad results at this station. We believe that the South America plate has continued to slide under the North Andes to this distance at 85 to 115 km depth. At 150 km depth, the velocity

quickly rises about 0.4 km/s where it stays until just below 215 km depth where it returns to the model. This is consistent with the edge of the northern slab described in Zarifi et al. (2007).

CONCLUSIONS

Not many 3-D models that can be directly compared to our data so asserting the correctness of the geologic analysis would be difficult. Other studies of Colombia have focused on this region in much different scales and areas without much exactness on their depths and locales. Using our data sets and techniques, we believe our data to have some consistencies with recent and past models of Colombia. Notable features we found in this research that can be comparable to others would be the presence of plates in the upper mantle at appropriate depths.

We believed to have seen the major plates beneath the North Andes plate. At about 60 km depth across the North Andes – South America plate boundary, we see a very shallow subduction that continues for a few hundred kilometers. We believe to have seen the deep slabs that are causing the Bucaramanga Nest seismicity that had been studied in Zarifi et Al (2007). The Nazca plate can be below at our western stations. Along the subduction zone of the Caribbean plate beneath the North Andes plate, we saw steep subduction.

REFERENCES

Allenby, R. J., 1984. Andean Tectonics: Implications For Satellite Geodesy. *NASA Technical Memorandum,* September, Issue 86160, pp. 3-17.

Ammon, C., n.d. *PGplot Surface Wave Multiple Filter Analysis.* s.l.:Penn State.

ANSS Comprehensive Catalog, 2015. *Realtime Earthquake Data Sources & Contributing Networks of Magnitude >2.5 from January 1, 1980 to April 28, 2015.* s.l.:USGS.

Bezada, M. J., Levander, A. & Schmandt, B., 2010. Subduction in the southern Caribbean: Images from finite-frequency P wave tomography. *Journal of Geophysical Research,* Volume 115.

Bezada, M. J., Levander, A. & Schmandt, B., n.d. Subduction in the southern Caribbean: Images from finite-frequency P wave tomography. *Journal of Geophysical Research,* Volume 115.

Bird, P., 2003. An updated digital model of plate boundaries. *Geochemistry Geophysics Geosytems,* 14 March.4(3).

Burdick, L. J. & Langston, C. A., 1977. Modeling crustal structure through the use of converted phases in teleseismic body-wave forms. *Bulletin of the Seismological Society of America,* June, 67(3), pp. 677-691.

Cassidy, J. F., 1992. Numerical experiments in broadband receiver function analysis. *Bulletin of the Seismological Society of America,* June, Volume 82, pp. 1453-1474.

Freymueller, J. T., Kellogg, J. N. & Vega, V., 1993. Plate Motions in the North Andean Region. *Journal of Geophysical Research,* 10 December, 98(B12), pp. 21853-21863.

Google Inc., 2013. *Colombia.* s.l.:Google Earth.

Gurrola, H., Zou, Z. & Talavera, N., 2015. Using a Three-Component Distributed Array of Mixed, Horizontal, and Vertical Single- Component Seismometers to Produce a Receiver Function from a Short Deployment. *Seismological Research Letters,* January/February, 86(1), pp. 158-164.

Hayes, G. P., 2007. *Integrating Seismological and Tectonic Studies to Constrain Lithospheric Evolution at Complex Plate Boundaries,* s.l.: Pennsylvania State University.

Jepsen, D. C. & Kennett, B. L. N., 1990. Three Component Analysis of Regional Seismograms. *Bulletin of the Seismological Society of America,* December, Volume 80, pp. 2032-2052.

Julia, A., C.J., H. R. & Correig, M., 2000. Joint inversion of receiver function and surface wave dispersion observations. *Geophys. J. Int.,* Volume 142, p. 99–112.

Langston, C. A. & Burdick, L. J., 1977. Modeling crustal structure through the use of converted phases in teleseismic body-wave forms. *Bulletin of the Seismological Society of America,* June, 67(3), pp. 677-691.

M. P. Barmin, M. H. R. A. L. L., 2001. A Fast and Reliable Method for Surface Wave Tomography. *Pure and Applied Geophysics,* pp. 1351-1375.

Mann, P., 1995. *Geologic and Tectonic Development of the Caribbean Plate Boundary in Southern Central America.* Boulder(CO): The Gological Society of America, Inc..

Pennington, W. D., 1981. Subduction of the Eastern Panama Basin and seismotectonics of northwestern South America. *Journal of Geophysical Research,* 10 November.86(B11).

Porritt, R. W., Becker, T. W. & Monsalve, G., 2014. Seismic anisotropy and slab dynamics from SKS splitting recorded in Colombia. *Geophysical Research Letters,* Volume 41.

Prieto, G. A. et al., 2013. Seismic evidence for thermal runaway during intermediate-depth earthquake rupture. *Geophysical Research Letters,* Volume 40.

Shearer, P. M., 2009. *Introduction to Seismology.* 2nd Edition ed. Cambridge: Cambridge University Press.

Sosa, A. et al., 2014. 3-D structure of the Rio Grande Rift from 1-D constrained joint inversion of receiver functions and surface wave dispersion. *Earth and Planetary Science Letters,* Volume 402.

Sosa, A. et al., 2013. Constrained optimization framework for joint inversion of geophysical data sets. *Geophysical Journal Internationa,* 17 September, Volume 195, pp. 1745-1762.

Stein, S. & Wysession, M., 2003. *An Introduction to Seismology, Earthquakes, and Earth Structure.* Malden(MA): Blackwell Pub..

USGS , 2012. *Poster of the Seismicity of the Nazca Plate and South America.* [Online] Available at: http://earthquake.usgs.gov/earthquakes/eqarchives/poster/regions/nazca.php

USGS, 2012. *Caribbean Tectonic Summary: Poster of the Seismicity of the Caribbean Plate and Vicinity.* [Online]
Available at: http://earthquake.usgs.gov/earthquakes/eqarchives/poster/regions/caribbean.php

Vargas, C. A. & Mann, P., 2013. Tearing and Breaking Off of Subducted Slabs as the Result of Collision of the Panama Arc-Indenter with Northwestern South America. *Bulletin of the Seismological Society of America,* June, 103(3), pp. 2025-2046.

Wessel, P. et al., 2013. Generic Mapping Tools: Improved Version Released. *EOS,* 5 November, 94(45), pp. 409-410.

Wirth, E. A. & Long, M. D., 2012. Multiple layers of seismic anisotropy and a low-velocity region in the mantle wedge beneath Japan: Evidence from teleseismic receiver functions.

Zarifi, Z., Havskov, J. & Hanyga, A., 2007. An insight into the Bucaramanga nest. *Tectonophysics.*

Zhang, J. & Langston, C. A., 1995. Dipping Structure under Dourbes, Belgium, Determined by Receiver Function Modeling and Inversion. *Bulletin of the Seismological Society of America,* February, 85(1), pp. 254-268.

VITA

Nicholas Talavera received his bachelor of science in geophysics in May of 2014 from Texas Tech University. Nicholas works as a Research Scholor at Cyber-ShARE at The University of Texas at El Paso. Nicholas did his undergraduate thesis entitled Efficacy of Using a Short Deployment of a Single-Component Geophone Array to Create Receiver Functions in 2014. Nicholas coauthored a publication in the January/February 2015 issue of Seismological Research Letters entitled Using a Three-Component Distributed Array of Mixed, Horizontal, and Vertical Single-Component Seismometers to Produce a Receiver Function from a Short Deployment. Nicholas was awarded Outstanding Graduate Student in Geophysics for 2016.

Permanent address: 734 S Mesa Hills Dr. Apt. #16
El Paso, TX 79912

This thesis/dissertation was typed by Nicholas Alexander Talavera.